land

MDPI

Article

Investigating the Heterogeneity Effects of Urban Morphology on Building Energy Consumption from a Spatio-Temporal Perspective Using Old Residential Buildings on a University Campus

Jinhui Ma [1], Haijing Huang [1,2,*], Mingxi Peng [3] and Yihuan Zhou [1]

[1] School of Architecture and Urban Planning, Chongqing University, Chongqing 400045, China; mjh@stu.cqu.edu.cn (J.M.); 20231501005@stu.cqu.edu.cn (Y.Z.)
[2] Key Laboratory of New Technology for Construction of Cities in Mountain Area, Chongqing University, Chongqing 400045, China
[3] Faculty of Smart Urban Design, Chongqing Jianzhu College, Chongqing 400072, China; m_peng@cqjzc.edu.cn
* Correspondence: cqhhj@cqu.edu.cn

Abstract: The significant increase in building energy consumption poses a major challenge to environmental sustainability. In this process, urban morphology plays a pivotal role in shaping building energy consumption. However, its impact may exhibit latent heterogeneity due to differences in temporal resolution and spatial scales. For urban energy planning and energy consumption modeling, it is crucial to pinpoint when and where urban morphology parameters matter, an overlooked aspect in prior research. This study quantitatively explores this heterogeneity, utilizing a detailed dataset from old residential buildings within a university campus. Spatial lag models were employed for cross-modeling across various temporal and spatial dimensions. The results show that annual and seasonal spatial regression models perform best within a 150 m buffer zone. However, not all significant indicators fall within this range, suggesting that blindly applying the same range to all indicators may lead to inaccurate conclusions. Moreover, significant urban morphology indicators vary in quantity, category, and directionality. The green space ratio exhibits correlations with energy consumption in annual, summer, and winter periods within buffer zones of 150 m, 50~100 m, and 100 m, respectively. It notably displays a negative correlation with annual energy consumption but a positive correlation with winter energy consumption. To address this heterogeneity, this study proposes a three-tiered framework—macro-level project decomposition, establishing a key indicator library, and energy consumption comparisons, facilitating more targeted urban energy model and energy management decisions.

Keywords: energy consumption; urban morphology; old residential buildings; university campus; spatio-temporal heterogeneity

Citation: Ma, J.; Huang, H.; Peng, M.; Zhou, Y. Investigating the Heterogeneity Effects of Urban Morphology on Building Energy Consumption from a Spatio-Temporal Perspective Using Old Residential Buildings on a University Campus. *Land* **2024**, *13*, 1683. https://doi.org/10.3390/land13101683

Academic Editor: Elena Lucchi

Received: 13 September 2024
Revised: 7 October 2024
Accepted: 14 October 2024
Published: 15 October 2024

1. Introduction

As populations agglomerate and cities expand, urban energy consumption increases significantly. It now represents two-thirds of global energy consumption [1]. This exacerbates carbon emissions, posing substantial challenges to environmental sustainability [2,3]. The latest report from the Intergovernmental Panel on Climate Change (IPCC) once again underscores the urgency of "guidelines on dismantling the climate time bomb" [4]. Alarming findings reveal that adverse climate effects have surpassed initial expectations in both depth and severity. Furthermore, the global population is projected to reach 9.7 billion by 2050, with the majority residing in cities [5], increasing urban energy demands. The construction industry is a major contributor to urban carbon emissions, accounting for about 40% of global emissions [6]. This is expected to rise by 40% in the next two decades [7].

Therefore, finding solutions to reduce this energy consumption and enhance resource efficiency is crucial for climate and energy goals, as well as environmental sustainability [8].

Extensive research has focused on reducing building energy consumption (BEC), primarily at the individual building level [9]. Efficient design strategies for individual buildings typically revolve around three fundamental aspects. Firstly, optimizing thermal insulation and natural lighting involves adjusting key building parameters, such as the building shape coefficient (*BSC*), orientation angle (*OA*), number of floors (*NF*), floor area (*FA*), and the thermal properties of its envelope [10–12]. Secondly, passive building design incorporates the use of renewable natural resources, like solar energy, wind energy, and natural light [13]. Lastly, improving the efficiency of a building's environmental performance is accomplished by enhancing its equipment systems [14]. In China, various types of national energy-saving standards have provided robust guidance for early-stage building design in different regions [15–17].

While such efforts have shown promise, existing energy-saving standards for individual buildings do not adequately address the challenges of urban energy planning. In reality, urban-level building cluster energy consumption is not a simple sum of individual building energy use. Furthermore, it demands a consideration of the impact of urban spatial design [18]. Factors like mutual shading between buildings in clusters and localized microclimates within an urban neighborhood significantly affect BEC [19]. Research highlights that urban morphology significantly influences urban energy efficiency [20], potentially altering building energy needs by 10~30% [21]. Moreover, future urban development, whether incremental construction or existing stock renewal, will reshape urban design, directly impacting urban building energy consumption (UBEC). Thus, a comprehensive understanding of the relationship between urban morphology and energy usage is crucial for effective city-level policies to combat climate change.

Current research on the impact of urban morphology on BEC primarily focuses on urban density, geometric shape, and environmental configuration. Urban density, a central focus, is commonly used to assess land development intensity [22]. Ref. [23] demonstrated that a higher floor area ratio significantly reduces BEC for winter heating in extremely cold regions. Ref. [24] found that increased neighborhood density leads to higher electricity consumption in slab and tower apartments during the summer. Similarly, research in Seattle [25] revealed that annual energy consumption in multi-family housings decreases with higher horizontal density and smaller variations in building height. These findings illustrate the complex influence of urban morphology on BEC, encompassing spatial usage patterns, climatic conditions, and interactions among different urban densities. Furthermore, early geometric shape studies expanded upon and refined urban morphology typologies such as courtyard, point, and slab morphology [26,27]. However, recent research places greater emphasis on authentic urban morphology classifications representing diverse regions and historical contexts. These studies utilize Ladybug Tools for performance simulation and Wallacei for multi-objective optimization analysis, aiming to identify energy-efficient urban morphologies [9,28]. Lastly, environmental configuration also plays a crucial role in modifying BEC by altering microclimatic conditions. In Singapore, increasing factors such as tree density, height, and greenery density have been shown to reduce cooling loads and BEC by 5~10% [29]. Ref. [30] extracted 40 urban building–vegetation morphology prototypes in Nanjing, China, and a simulation revealed that, particularly in hot climate zones and hot summer/cold winter zones, avoiding low greenery and low-density urban morphologies is advisable. Hence, strategic urban morphology planning can significantly lower UBEC.

While progress has been made in related fields, obstacles still persist in bridging research findings with policy formulation [1]. The existing research gaps can be discussed as follows:

Controversy in Urban Morphology Effects: There is significant debate about how urban morphology affects BEC [22]. This stems largely from discrepancies in time and space resolution [31,32], making it difficult to compare research findings within the same dimension. Specifically, the influence of time on BEC has been underexplored [3]. For

instance, Ref. [25] investigated the effects of horizontal compactness, vertical density, and variations in building height on the annual energy consumption of multifamily housing. Ref. [23] primarily focused on the relationship between urban morphology and winter heating energy consumption in cold regions. Ref. [29] investigated the effects of variations in urban form—specifically density, height, and greenery density—during the summer, based on a comprehensive analysis of 32 real-world cases representing different urban morphologies. Whether this relationship varies seasonally remains uncertain. Additionally, there is no consensus on the scale at which urban morphology significantly impacts BEC. Ref. [33] found that, within a 50 m buffer zone, the regression coefficient of urban form and building energy consumption in Singapore is relatively high. In a study from Seattle [25], it was shown that the correlation between urban form and energy consumption is strongest within a 100 m buffer zone. Similarly, Ref. [34] used multiple linear regression to discover that at the block scale, the regression model's R-squared value is maximized within a 100 m buffer zone in Harbin, China. However, earlier studies in cold regions employed a 150 m buffer zone for modeling [23]. Clearly defining the spatial boundaries for key urban morphology parameters and their corresponding energy consumption periods is crucial when developing comprehensive energy planning tools [35].

Reliance on Simulated Data: Most studies rely on simulated building energy data, which diminishes the credibility of their findings in policymaking. Building simulation research relies on detailed information about building composition to establish dynamic heat transfer models based on thermodynamic principles, enabling the calculation of building performance [36]. Traditional building simulation primarily focuses on individual physical buildings and does not take into account their surrounding environment [37]. In fact, when the subject shifts from individual buildings to urban building clusters, the entire energy consumption simulation requires substantial computational resources and time [38]. This also involves the dual diversity of building types and human behavior [39]. The energy consumption simulation models inherently exhibit uncertainty, thus often failing to precisely depict the actual energy consumption scenario [40]. The challenge lies in acquiring detailed basic building data and actual energy usage data for urban energy models [41]. Gathering these extensive data involves time-consuming efforts and raises privacy and security concerns [42]. Nonetheless, the use of genuine and effective building energy data remains crucial for accurately reflecting real conditions and enhancing research reliability [39].

Overlooking Urban Climate: Even within the same city, localized climate variations have a substantial impact on BEC [43]. This aspect has often been ignored in previous studies [23,25], which focused on collecting building samples at a broader urban scale, inevitably giving rise to potential climatic disparities.

Given the identified research gaps, this study aims to provide more empirical evidence regarding the potential heterogeneous impacts of neighborhood-scale urban morphology on BEC at different temporal and spatial resolutions within real geographical contexts. Few studies have previously explored the interaction between urban morphology and BEC simultaneously in both temporal and spatial dimensions. To achieve research goals, this study prioritized ensuring the consistency of variables other than urban morphology when selecting sample buildings. Hence, a detailed dataset was constructed using old residential buildings within a university campus, encompassing integrated basic building data, urban morphology data, and real BEC data. These buildings share similar occupant profiles, income levels, education, daily routines, and are subject to the same energy policies and electricity pricing. Crucially, they are all located in the same geographic region, ensuring consistent urban climate and avoiding the influence of local climate variations. Our study aims to answer the following questions to enhance the empirical understanding of how urban morphology at different scales affects residential energy consumption across different time periods:

(1) After controlling for variations in a building's basic information, local climate, and behavioral and socioeconomic factors, does the neighborhood-scale urban morphology in mountainous cities correlate with BEC? How does it differ from other cities?
(2) Does the impact of urban morphology on BEC maintain consistency across different spatial scales within the same timeframe? If not, how does this heterogeneity manifest?
(3) Within the same spatial scale, do the effects of urban morphology on BEC vary during different time periods, including the entire year, summer, and winter?

2. Materials and Methods

2.1. The Framework of This Study

Figure 1 presents the three main steps of our study.

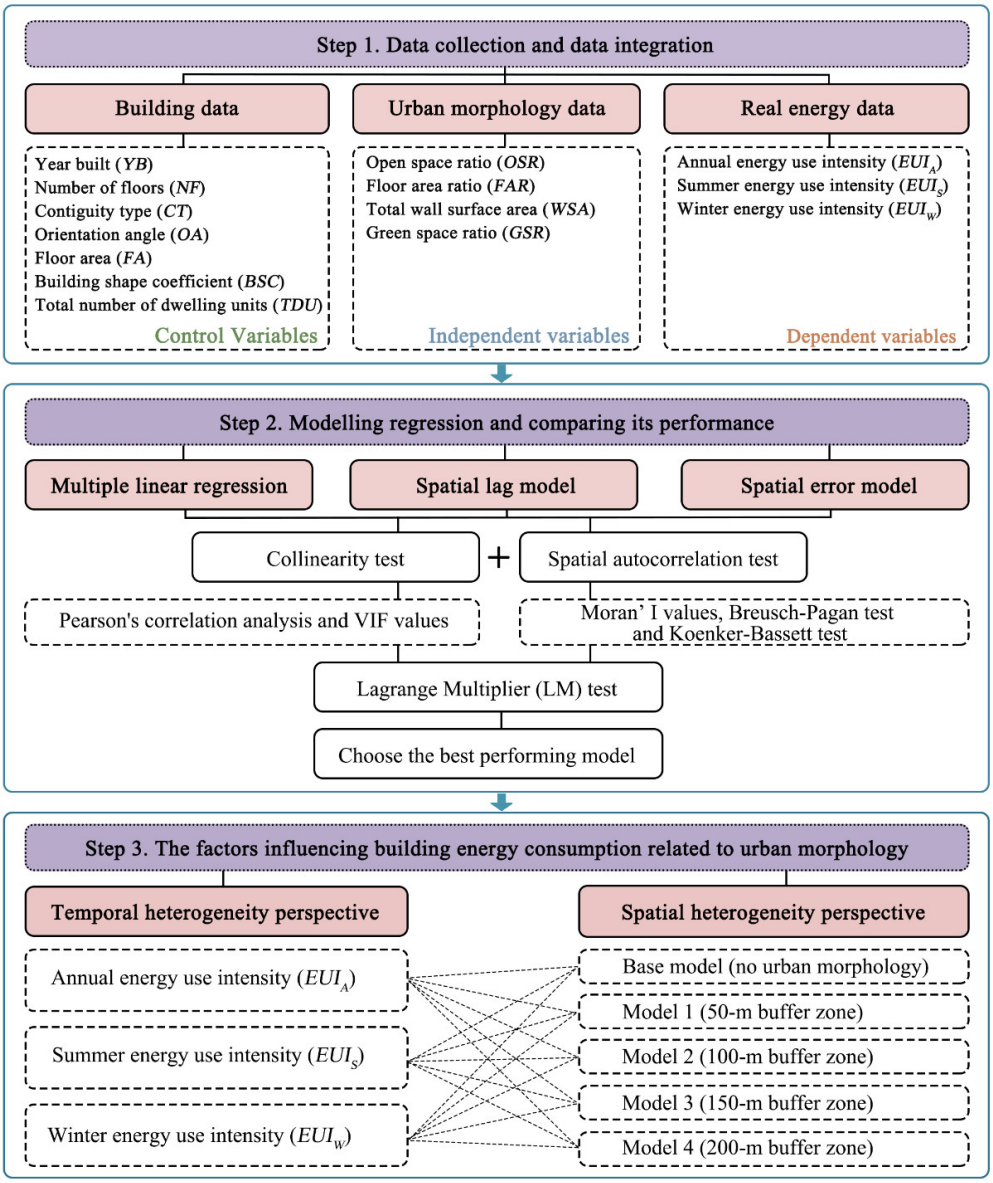

Figure 1. Research framework.

- Step 1—data collection and integration: This study utilized ArcGIS 10.8 to construct a database integrating basic building data, urban morphology data, and actual BEC data. Building foundational data served as a control variable, while urban morphology data at various spatial scales acted as independent variables, and actual BEC data acted as the dependent variable, ensuring study comparability, reliability, and completeness.

- Step 2—comparative regression model analysis: Three types of regression models were employed to quantify urban morphology's impact on BEC. Model applicability was assessed through multicollinearity tests and spatial autocorrelation analysis. Lagrange multiplier (LM) tests were used to select the model with the best fit and explanatory power.
- Step 3—urban morphology's impact on BEC: We cross-modeled BEC at different time periods with urban morphology at various spatial scales using the selected model from Step 2. In each group, a base model was established, not accounting for spatial morphology. Comparative analysis with the base model enables a more objective evaluation of urban morphology's spatio-temporal heterogeneous effects on BEC.

2.2. Study Area

The research site is Chongqing, known as one of China's "Four Furnace" cities, located between 105°17′ to 110°11′ east longitude and 28°10′ to 32°13′ north latitude in Figure 2. As one of China's four directly administered municipalities, Chongqing boasts varying elevations ranging from 73 to 2797 m, making it the largest mountainous city in China. According to the Koppen–Geiger climate classification [44], it falls into the C_{wa} and C_{fa} climate zones, classified as subtropical humid climates, with an annual average dry-bulb temperature of 27.8 °C. The hottest and coldest months typically reach an average of 36.4 °C in summer and 3 °C in winter. According to the Chinese standard *GB 50176-2016 Code for Thermal Design of Civil Building* [17], Chongqing's climate is categorized as a hot summer/cold winter zone, resulting in significant cooling and heating demands for its buildings.

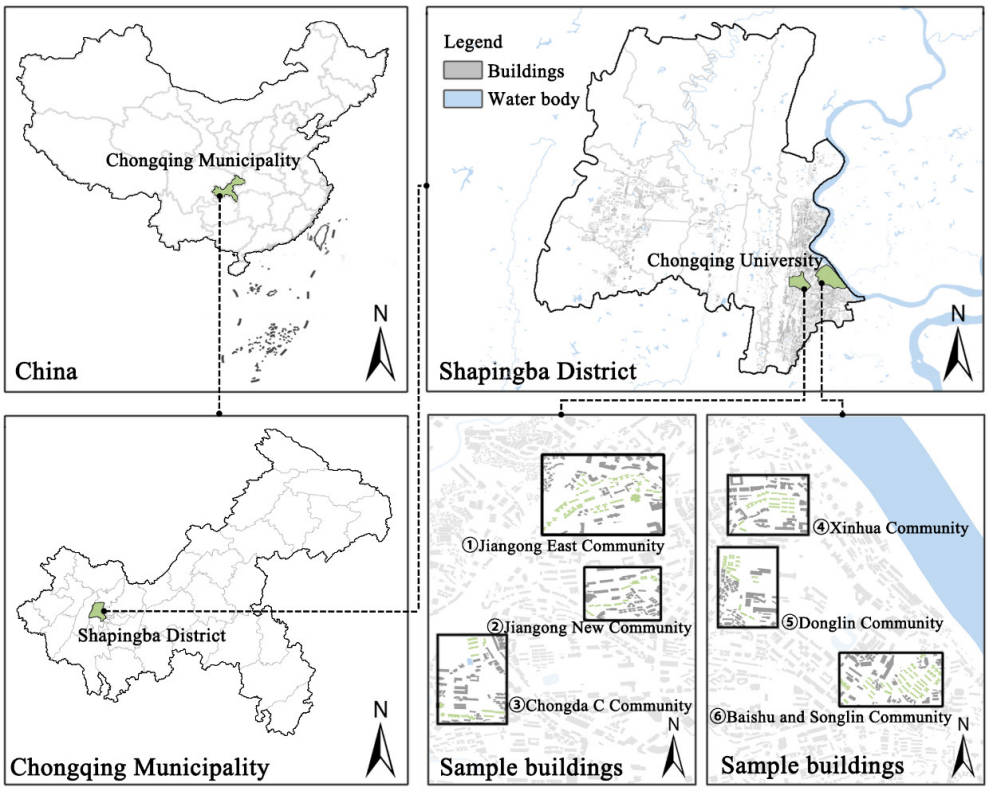

Figure 2. Study area and sample residential buildings.

2.3. Data Preparation

2.3.1. Using Basic Building Data as Control Variables

Differing from on-site measurements, this research obtained highly precise basic building data from construction blueprints, exclusively sourced from the Infrastructure Office of Chongqing University. This approach significantly assures the authenticity, accuracy, and reli-

ability of the data. Previous studies in the literature indicate that the physical characteristics of buildings are closely related to BEC [45–47]. Therefore, exploring the significance of urban morphological variables at the neighborhood scale on BEC requires consideration of the physical features of buildings. Seven key building attributes were selected as control variables: year built (*YB*), contiguity type (*CT*), *NF*, *OA*, *FA*, *BSC*, and total number of dwelling units (*TDU*). These control variables can adequately reflect the morphological and performance characteristics of the buildings themselves. Specifically, *YB* signifies the construction period, reflecting envelope structure characteristics and heating system efficiency. Evolving building energy regulations in China have influenced residential envelope design over different periods,[1] resulting in some consistency in envelope structure characteristics within the same era [23,51]. Regarding building morphology, *CT* is a significant factor influencing BEC [52]. Housing types were categorized into detached, row, and staggered layouts [10]. A larger *BSC* implies a greater surface area for the same building volume, leading to increased heat dissipation and higher BEC, making it less energy efficient. Additionally, previous studies in the literature have widely reported the significant impact of residential building area on household electricity consumption, with larger residential areas generally leading to higher absolute electricity usage [10,25,53,54]. Therefore, variables such as the *NF*, *FA*, and *TDU* are also considered. We selected *OA* as a supplement to building morphology, as south-facing buildings (in the Northern Hemisphere) typically receive more sunlight, which aids in passive solar heating during winter but may increase cooling loads in summer. For detailed descriptions of these variables, refer to Table 1.

Table 1. Description of selected variables.

Data	Raw Data	Unite	Description	Formula (or Data Processing)	Data Source	References
Energy use intensity	Annual electricity usage (EUI_A)	kWh/m^2	Annual electricity consumption per unit area of sample buildings.	$EUI_A = (E_A/12)/A_{GF}$, where E_A is the total annual electricity consumption, and A_{GF} is the gross floor area.	Chongqing University Energy Conservation Office	[24]
	Summer electricity usage (EUI_S)	kWh/m^2	Summer electricity consumption per unit area of sample buildings.	$EUI_S = (E_S/3)/A_{GF}$, where E_S is the total summer electricity consumption.	Chongqing University Energy Conservation Office	[24]
	Winter electricity usage (EUI_W)	kWh/m^2	Winter electricity consumption per unit area of sample buildings.	$EUI_W = (E_W/3)/A_{GF}$, where E_W is the total winter electricity consumption.	Chongqing University Energy Conservation Office	[24]
Basic building information	Year built (*YB*)	Year	Sample buildings' age	$YB = Y_i - Y_C$, where Y_i is the current year, and Y_C is the construction year.	Infrastructure Office of Chongqing University	[55]
	Number of floors (*NF*)	Story	Number of floors in the sample buildings.	Count the number of floors for sample buildings based on the construction design drawings.	Infrastructure Office of Chongqing University	[11,12]
	Contiguity type (*CT*)	-	Contiguity type of the sample buildings.	Determined based on sample building plan form: "0" represents a detached house with no contiguity; "1" represents a row house with one common boundary; "2" represents a staggered house with two boundaries.	Infrastructure Office of Chongqing University	[10]
	Orientation angle (*OA*)	°	Orientation angle of the sample buildings.	The building facing directly south is considered 0 degrees. Calculate the angle formed between the building's orientation and due south.	Infrastructure Office of Chongqing University	[56,57]
	Floor area (*FA*)	m^2	Average floor area of the sample buildings.	Calculate the average floor area for sample buildings based on the construction design drawings.	Infrastructure Office of Chongqing University	[53]
	Building shape coefficient (*BSC*)	m^{-1}	The ratio of the exterior surface area in contact with outdoor air to the enclosed volume.	$BSC = (A_f + A_r)/V$, where A_f is the facade area, A_r is the roof area, and V is the volume.	Infrastructure Office of Chongqing University	[58,59]
	Total number of dwelling units (*TDU*)	-	Number of households inside the sample buildings.	Conduct a survey of residential households in sample buildings based on the construction design drawings.	Infrastructure Office of Chongqing University	[25,54]

Table 1. Description of selected variables.

Data	Raw Data	Unite	Description	Formula (or Data Processing)	Data Source	References
Urban morphology information	Open space ratio (*OSR*)	Ratio	Reflecting the degree of land development for the buildings.	$OSR = 1 - A_{fp}/A_d$, where A_{fp} is the footprint area, and A_d is the sample district (buffer zone) area.	Gaode map	[60]
	Floor area ratio (*FAR*)	Ratio	Reflecting the openness of the two-dimensional space around the buildings.	$GSR = A_{gf}/A_d$, where A_{gf} is the sum of the areas of all building floors.	Gaode map	[60]
	Total wall surface area (*WSA*)	km^2	Sum of the exposed surface area to air of all buildings within the plots, excluding the sample buildings.	$WSA = \sum_{i=1}^{n} A_{fi} + A_{ri}$, where A_{fi} is the facade area of building i in the buffer zone, and A_{ri} is the roof area of building i in the buffer zone.	Gaode map	[23]
	Green space ratio (*GSR*)	Ratio	Reflecting the level of green construction.	$GSR = A_{gg}/A_d$, where A_{gg} is the gross green space area in the buffer zone.	Urban green space dataset	[25]

2.3.2. Utilizing Urban Morphology Data as Independent Variables

In contrast to flat cities with grid-like road networks, Chongqing's buildings have a fragmented spatial layout [61]. Therefore, most of the old residential buildings constructed before 2000 in Chongqing do not have specific regular patterns or clusters. Previous studies in other climatic regions typically define the scale of block morphology within a range of 50 to 200 m [25,62]. Within this range, urban morphology can significantly influence the urban thermal environment, which is a primary factor contributing to differences in building energy consumption. To analyze the surrounding urban morphology, this study created circular buffers around the sample buildings with radii ranging from 50 to 200 m to assess the impact of urban morphology at various spatial scales in Figure 3. Vector graphic information, including building base outlines and the number of floors, was extracted from the Gaode Map. Subsequently, graphic corrections were conducted using GIS to obtain morphological data for the building cluster. Green morphology data were sourced from the high-resolution Urban Green Space dataset (UGS-1m), generated through deep learning on Google Earth imagery [63]. This 1 m resolution data provided enhanced accuracy.

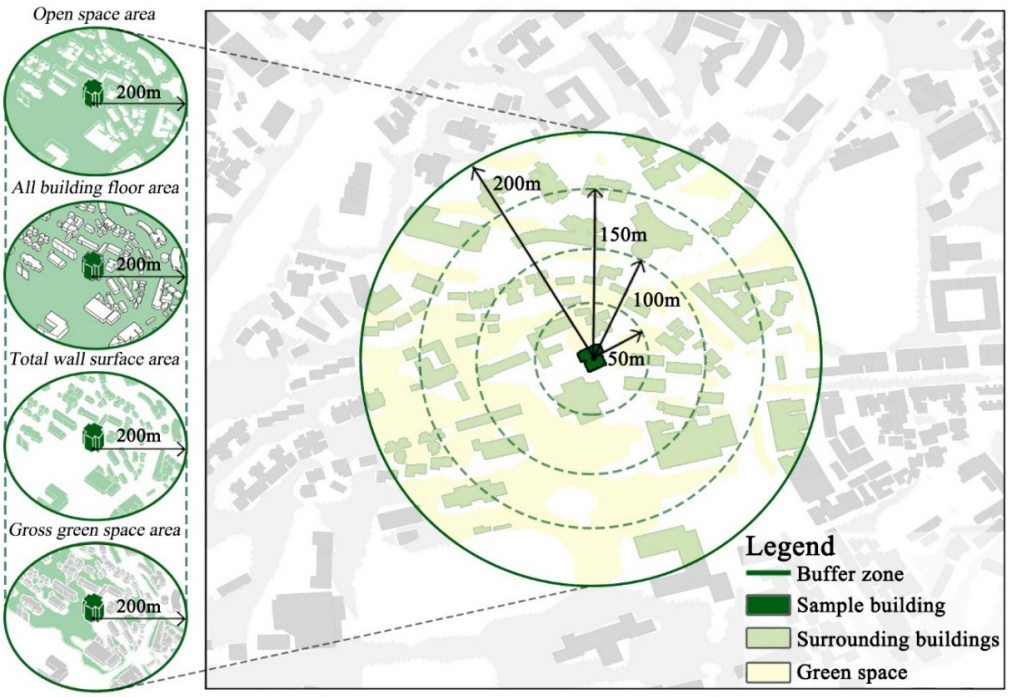

Figure 3. Establishing buffers of different spatial scales around the sample buildings.

This study employed four indicators—open space ratio (*OSR*), floor area ratio (*FAR*), total wall surface area (*WSA*), and green space ratio (*GSR*)—to describe urban morphology, as they influence heat island intensity, ventilation efficiency, and radiation effects, consequently affecting BEC [3]. *OSR* reflects two-dimensional space openness around buildings, with higher values indicating lower horizontal compactness. *FAR* indicates overall land development level, with higher values indicating greater building density nearby. *WSA* captures three-dimensional building group morphology, especially vertical compactness, while *GSR* reflects green construction's impact on the microclimate and BEC. The specific formulas for these urban morphology indicators are detailed in Table 1.

2.3.3. Computing Building Energy Consumption as the Dependent Variable

This study obtained prior authorization from the Chongqing University Energy Conservation Office, enabling us to access water, electricity, and gas consumption data for all users (5521 households). The heating system in China differs significantly from those in other countries worldwide. In the 1950s, the central government established a north–south heating boundary line across the nation, with regions south of this line refraining from centralized heating systems. Despite the cold and humid winters in Chongqing, the centralized heating system did not gain traction, especially in these old residential buildings. Therefore, in this study, the samples still rely on electricity as their primary fuel source, using air conditioning predominantly for heating in winter. Summer electricity consumption was calculated based on household electricity usage data from June to September 2015, while winter electricity consumption was determined using data from December 2014 to February 2015. Since 2014, these old buildings and their surrounding environments have remained unchanged, ensuring that the electricity consumption, environmental, and building data used in this study are fully compatible.

Traditionally, most studies use electricity consumption per unit building area or volume to assess building energy usage intensity (EUI). Considering that the building heights of most sampled structures before 2000 primarily ranged from 2.8 to 3 m, and in light of the statistical consistency in the number of occupants per unit of building area, the average monthly electricity consumption per unit of building area was employed as the indicator for EUI. Its credibility and reliability have been thoroughly substantiated in prior research [64].

Datasets often contain missing values and outliers. This study replaced missing values with the mean value of the respective attribute [65]. Additionally, outliers can distort research results. We used the box plot method, which is suitable for detecting outliers in samples with unknown distribution shapes [66]. Outliers were categorized as mild or extreme, as shown in Figure 4. To mitigate the impact of individual extreme users on BEC while ensuring sample representativeness, extreme outliers were identified and removed. Table 2 provides descriptive statistics for all variables after processing.

To further validate the processed data, this study categorized the construction years of older residential buildings into four periods, 1949~1985, 1986~1992, 1993~2000, and 2001~2010, based on the release of China's energy-saving design standards. The statistics of EUI for different construction periods are depicted in Figure 5. The order of median and mean values, from highest to lowest, follows this pattern: Summer energy usage intensity (EUI_S) > Winter energy usage intensity (EUI_W) > Annual energy usage intensity (EUI_A), consistent with the BEC pattern in hot summer/cold winter zones. Comparing the four periods, buildings constructed between 1949 and 1985 exhibit significantly higher median and mean energy intensity values. As mentioned in Section 2.3.1, energy efficiency was not a consideration in the design of buildings during this period. Subsequently, energy-saving requirements improved with each iteration of China's building energy-saving regulations, leading to continuous enhancements in building envelope thermal insulation performance. Consequently, EUI_A, EUI_S, and EUI_W all exhibit a clear decreasing trend over time. These analyses affirm the credibility and reliability of the processed dataset regarding BEC.

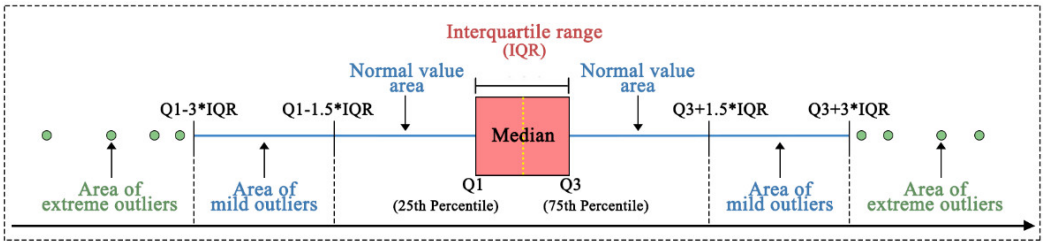

Figure 4. Box plot method to identify anomalous data.

Table 2. Descriptive statistics of the variables.

Variable Type	Variables	Mean	Standard Deviation	Minimum	Maximum
Dependent Variable	EUI_A (kWh/m^2)	2.01	0.62	0.44	4.26
	EUI_S (kWh/m^2)	2.87	0.96	0.57	6.20
	EUI_W (kWh/m^2)	2.14	0.76	0.51	4.68
Control Variable	*YB* (year)	38.79	10.84	20	70
	NF (number)	7.21	4.53	2.00	32.00
	CT	0.87	0.67	0	2
	OA (°)	20.50	19.74	0	87.00
	FA (m^2)	354.07	224.33	94.35	1274.77
	BSC (m^{-1})	0.39	0.08	0.15	0.63
	TDU (number)	40.60	35.49	4	256
Urban Morphology Variable	*OSR* in 50 m buffer zone (%)	0.75	0.07	0.33	0.87
	FAR in 50 m buffer zone (%)	2.92	2.18	0.96	13.39
	WSA in 50 m buffer zone (km^2)	0.04	0.02	0.01	0.10
	GSR in 50 m buffer zone (%)	0.49	0.18	0.03	0.92
	OSR in 100 m buffer zone (%)	0.76	0.05	0.62	0.90
	FAR in 100 m buffer zone (%)	3.34	1.34	0.60	7.16
	WSA in 100 m buffer zone (km^2)	0.17	0.06	0.03	0.33
	GSR in 100 m buffer zone (%)	0.47	0.14	0.17	0.84
	OSR in 150 m buffer zone (%)	0.76	0.04	0.67	0.88
	FAR in 150 m buffer zone (%)	3.81	1.29	1.25	7.09
	WSA in 150 m buffer zone (%)	0.40	0.13	0.16	0.77
	GSR in 150 m buffer zone (%)	0.44	0.11	0.22	0.77
	OSR in 200 m buffer zone (%)	0.76	0.03	0.69	0.86
	FAR in 200 m buffer zone (%)	3.93	1.06	1.80	6.38
	WSA in 200 m buffer zone (km^2)	0.74	0.20	0.36	1.25
	GSR in 200 m buffer zone (%)	0.43	0.08	0.28	0.62

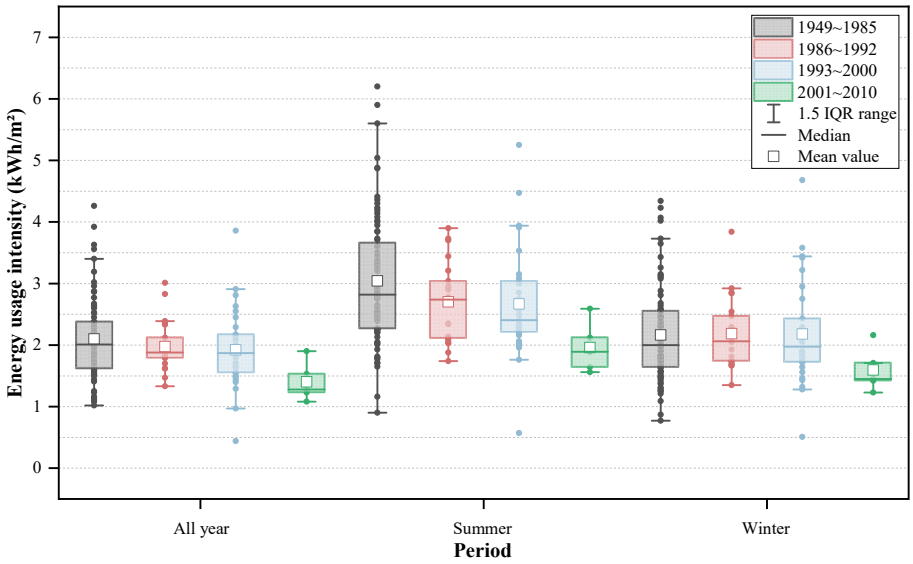

Figure 5. Energy consumption intensity of the sample residential buildings at different time periods.

2.4. Regression Models

To ensure the appropriateness and robustness of the model, multiple linear regression (MLR), spatial lag models (SLMs), and spatial error models (SEMs) were selected to quantify the impact of urban morphology on BEC. These are the most favored regression algorithms in related research [25,39,67].

Spatial autocorrelation refers to the potential interdependence among observed data within the same distribution area [68,69]. Using statistical models that do not account for the effects of spatial autocorrelation may lead to biased results and erroneous inferences [70], which has been a limitation in previous energy research [71]. Hence, considering the possible presence of spatial autocorrelation in EUI, we calculated the Moran's I statistic for the dependent variable, as expressed in Equation (1):

$$\text{Moran's } I = \frac{\sum_{i=1}^{n}\sum_{j=1}^{m} w_{ij}(x_i - \overline{x})(x_j - \overline{x})}{S^2 \sum_{i=1}^{n}\sum_{j=1}^{m} W_{ij}} \quad (1)$$

where x_i and x_j represent the observed values of a specific attribute within spatial units i and j, respectively, S^2 is the variance, and W_{ij} is the spatial weighting values, which form the W matrix (n*n).

This study employs Geoda and SPSS to execute our model, following these key steps. First, we select appropriate variables. Next, we execute multiple linear regression (MLR) and scrutinize model collinearity using Pearson correlation analysis and variance inflation factor (VIF) assessment. We then determine statistical significance regarding spatial autocorrelation based on Moran's I value. Following this, we assess the need for a spatial regression model based on the results of the Breusch–Pagan and Koenker–Bassett tests, if non-significant. After that, we evaluate the performance of the Spatial Lag Model (SLM) and Spatial Error Model (SEM) via LM comparison. Finally, we select the optimal-performing model for further analysis. Detailed descriptions of the three regression models are presented as follows.

The formula for the MLR can be expressed as Equation (2):

$$EUI = \beta_0 + \beta_1 x_1 + \beta_2 x_2 + \ldots + \beta_p x_p + \varepsilon \quad (2)$$

where EUI is the energy use intensity for summer, winter, and all year round, β_0 is the general model intercept, β_i is the regression coefficient (i = 1, 2, …, p), x_i is the input variables, and ε is the error term.

If there exists significant spatial autocorrelation in the dependent variable, it becomes imperative to engage in spatial regression analysis. The SLM is represented as Equation (3):

$$EUI = \rho W_{EUI} + \beta X + \varepsilon, \varepsilon \sim \left(0, \delta^2 I_n\right) \quad (3)$$

where ρ is the spatial lag coefficient, W_{EUI} is the spatial weights matrix, X is the matrix of independent variables, β is the vector of coefficients for the independent variables, and ε is the stochastic error.

The SEM is depicted as Equation (4):

$$EUI = \beta X + \lambda W_{\mu} + \varepsilon, \varepsilon \sim \left(0, \delta^2 I_n\right) \quad (4)$$

where λ is the spatial error factor, and W_{μ} is the spatial weight matrix.

To facilitate comparative analysis, the regression models for various urban scales (50 m, 100 m, 150 m, and 200 m buffers) are labeled as Model 1, Model 2, Model 3, and Model 4, respectively. By contrasting these models with the base model, which does not account for spatial morphology, we can objectively evaluate the spatio-temporal heterogeneity effects of urban morphology on BEC.

3. Results and Discussion

3.1. Results of Multicollinearity Analysis

This study employs Pearson correlation analysis to initially identify linear relationships between pairs of variables (Figure 6). Pearson correlation coefficient *r* quantifies the degree of association, with *r* greater than 0 indicating a positive relationship and r less than 0 indicating a negative relationship. Overall, for Model 1, Model 2, Model 3, and Model 4, the absolute range of Pearson's *r* values falls between 0 and 0.6, with proportions of 92.8%, 94.5%, 92.8%, and 92.8%, respectively. This suggests that only a small subset of pairwise variables exhibits strong localized correlations. However, it is essential to note that the correlation between two independent variables does not comprehensively address multicollinearity. Therefore, a more comprehensive assessment of multicollinearity is conducted using the VIF. Table 3 presents the results of the multicollinearity tests for each model, revealing that all variables across the four model categories have VIF values well below the threshold of 10. Combining the outcomes from both analyses, it is concluded that there is no significant multicollinearity among pairwise variables in the variable pool. Consequently, no variables need to be removed at this stage of our investigation.

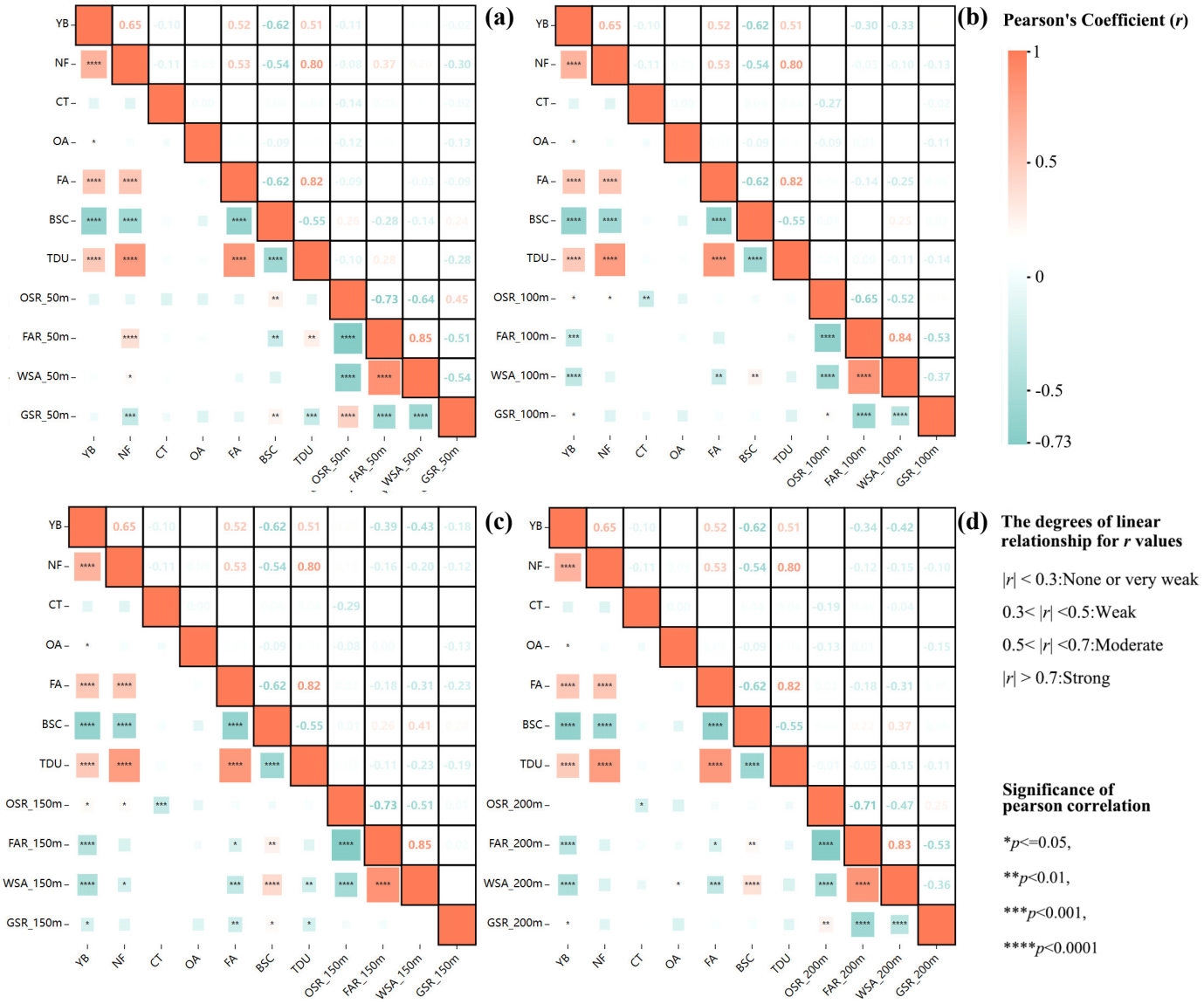

Figure 6. Pearson correlation results: (**a**) Model 1, (**b**) Model 2, (**c**) Model 3, and (**d**) Model 4.

Table 3. Collinearity test results.

Variables	Model 1 (50 m Buffer Zone)		Model 2 (100 m Buffer Zone)		Model 3 (150 m Buffer Zone)		Model 4 (200 m Buffer Zone)	
	TOL	VIF	TOL	VIF	TOL	VIF	TOL	VIF
YB	0.362	2.760	0.348	2.871	0.356	2.811	0.316	3.166
NF	0.167	5.984	0.178	5.606	0.172	5.820	0.176	5.685
CT	0.896	1.116	0.868	1.153	0.860	1.162	0.867	1.154
OA	0.876	1.142	0.847	1.181	0.774	1.292	0.581	1.722
FA	0.193	5.193	0.194	5.144	0.200	4.995	0.189	5.277
BSC	0.435	2.301	0.447	2.239	0.418	2.394	0.392	2.548
TDU	0.118	8.445	0.119	8.429	0.118	8.474	0.117	8.542
OSR	0.348	2.878	0.419	2.389	0.331	3.023	0.286	3.497
FAR	0.143	7.003	0.156	6.425	0.133	7.531	0.084	7.822
WSA	0.201	4.975	0.245	4.076	0.182	5.488	0.150	6.673
GSR	0.539	1.857	0.569	1.757	0.892	1.121	0.430	2.326

Note: TOL means tolerance. VIF means variance inflation factor.

3.2. Regression Model Performance Comparison and Selection

According to Figure 7a–c, global Moran's I calculation results corresponding to EUI_A, EUI_S, and EUI_W are 0.458, 0.371, and 0.494, respectively. Following the Breusch–Pagan test and Koenker–Bassett test, it is observed that all model *p*-values exceed 0.05. This signifies a significant spatial autocorrelation for EUI_A, EUI_S, and EUI_W, implying a potential risk of error when employing MLR models for regression analysis. Therefore, the SLM and SEM are utilized to address this issue [61].

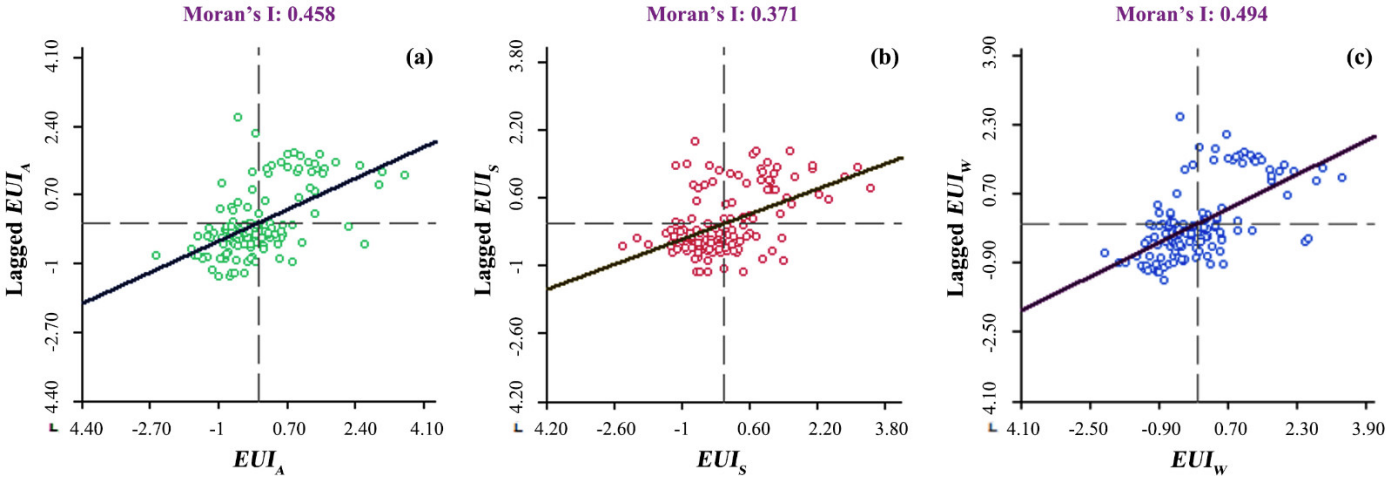

Figure 7. Result of Moran's I for the (**a**) EUI_A, (**b**) EUI_S, and (**c**) EUI_W of sample residential buildings.

To select models with superior explanatory power and fit, this paper conducted a statistical evaluation of all cross-regression results for SLM and SEM. Table 4 summarizes statistically significant indicators for spatial regression performance comparison. Notably, the LM test emphasizes that all 12 regression results of SLM exhibit significant performance. Conversely, for EUI_A, SEM's Model 2 and Model 3 regression results lack significance. Furthermore, the overall significance of SEM is notably lower than that of SLM for EUI_S. In addition, SLM, as a whole, boasts higher LM values compared to SEM, signifying superior model fitting and explanatory capabilities. Finally, when comparing the models using the Akaike Information Criterion (AIC) and Schwarz Criterion (SC), lower AIC and SC values suggest a model's ability to more accurately represent reality [72]. Consequently, SLMs with smaller AIC values demonstrate higher precision in comparison to SEMs. Overall, SLM was selected to investigate the influence of urban morphological variables on EUI.

Table 4. Comparison of regression results between SLM and SEM.

Energy Consumption	Model Type	LM Value		SC		AIC	
		SLM	SEM	SLM	SEM	SLM	SEM
EUI_A	Model 1 (50 m buffer zone)	20.69 **	5.17 *	916.99	921.20	879.12	886.25
	Model 2 (100 m buffer zone)	17.40 **	3.59	914.08	917.61	876.21	882.66
	Model 3 (150 m buffer zone)	17.93 **	3.33	910.22	914.62	872.35	879.67
	Model 4 (200 m buffer zone)	21.31 **	7.07 **	913.77	915.70	875.90	880.75
EUI_W	Model 1 (50 m buffer zone)	28.80 **	11.80 **	601.76	603.60	563.89	568.65
	Model 2 (100 m buffer zone)	20.99 **	7.55 **	597.53	599.97	559.67	565.01
	Model 3 (150 m buffer zone)	25.80 **	9.85 **	594.40	599.02	556.53	564.07
	Model 4 (200 m buffer zone)	35.13 **	15.71 **	600.10	601.06	562.24	566.11
EUI_S	Model 1 (50 m buffer zone)	12.71 **	3.97 *	672.39	672.51	634.53	637.56
	Model 2 (100 m buffer zone)	14.58 **	5.32 *	673.48	673.12	635.62	638.17
	Model 3 (150 m buffer zone)	14.38 **	5.72 *	667.07	667.91	629.20	632.96
	Model 4 (200 m buffer zone)	18.88 **	14.05 **	669.58	669.23	631.71	634.29

Note: (1) LM means Lagrange multiplier. SC means Schwarz criterion. AIC means Akaike info criterion. (2) * $p < 0.05$, ** $p < 0.01$. (3) The darker the color the better the performance of the model.

3.3. Regression Results

After including spatial lag variables within the control variables, Tables 5–7 display the regression results for EUI_A, EUI_S, and EUI_W. Each set of regressions includes five SLMs that examine the relationships between various scales of urban morphology and BEC. In each set of regression results, the base model includes only basic building variables. Models 1, 2, 3, and 4 then add urban morphological indicators within 50 m, 100 m, 150 m, and 200 m buffer zones as explanatory variables. Overall, the inclusion of urban morphological indicators leads to improved model fit for EUI_A, EUI_S, and EUI_W.

Table 5. Comparison of regression results from spatial lag models of EUI_A.

Variable	Base Model		Model 1 (50 m Buffer Zone)		Model 2 (100 m Buffer Zone)		Model 3 (150 m Buffer Zone)		Model 4 (200 m Buffer Zone)	
	Coefficient	*z*-Value	Coefficient	*z*-Value	Coefficient	*z*-Value	Coefficient	*z*-Value	Coefficient	*z*-Value
Spatial lag	0.419 **	4.843	0.366 **	4.069	0.338 **	3.661	0.306 **	3.219	0.306 **	3.109
Constant	−73.811	−0.540	−4.455	−0.031	27.860	0.191	6.592	0.045	57.308	0.709
YB	0.053	0.764	0.019	0.260	0.021	0.281	0.036	0.504	0.003	0.042
NF	−0.716 **	−2.983	−0.707 **	−2.755	−0.575 *	−2.338	−0.736 **	−2.970	−0.685 **	−2.766
CT	1.621 *	2.153	1.853 *	2.441	1.699 *	2.213	1.684 *	2.232	1.615 *	2.118
OA	0.042	1.655	0.061 *	2.357	0.058 *	2.279	0.014	0.526	0.040	1.301
FA	−0.020 **	−4.182	−0.023 **	−4.772	−0.022 **	−4.618	−0.021 **	−4.606	−0.022 **	−4.463
BSC	28.209 **	3.194	33.472 **	3.621	31.790 **	3.539	32.210 **	3.527	32.506 **	3.409
TDU	0.107 **	2.756	0.122 **	3.132	0.111 **	2.908	0.118 **	3.097	0.118 **	3.060
OSR			−2.376	−0.216	−26.265	−1.624	−46.585 *	−2.146	−40.176	−1.479
FAR			0.550	0.958	0.636	0.719	3.542 **	3.366	2.252	1.423
WSA			−62.660	−1.092	8.590	0.577	26.066 **	3.063	7.464	1.227
GSR			−6.492	−1.779	−9.361 *	−2.020	−8.724 *	−1.988	−11.919	−1.356
R-squared	0.433		0.450		0.458		0.472		0.457	
LL	−429.441		−426.561		−425.106		−423.176		−424.951	

Note: (1) LL means log likelihood; (2) * $p < 0.05$, ** $p < 0.01$.

Table 6. Comparison of regression results from spatial lag models of EUI_S.

Variable	Base Model		Model 1 (50 m Buffer Zone)		Model 2 (100 m Buffer Zone)		Model 3 (150 m Buffer Zone)		Model 4 (200 m Buffer Zone)	
	Coefficient	*z*-Value	Coefficient	*z*-Value	Coefficient	*z*-Value	Coefficient	*z*-Value	Coefficient	*z*-Value
Spatial lag	0.385 **	4.261	0.330 **	3.522	0.337 **	3.570	0.330 **	3.486	0.325 **	3.355
Constant	21.271	0.381	40.742	0.688	71.482	1.178	53.102	0.895	75.503	1.213
YB	−0.006	−0.200	−0.016	−0.545	−0.030	−0.985	−0.118	0.604	−0.033	−1.056
NF	−0.275 **	−2.818	−0.288 **	−2.752	−0.237 *	−2.335	−0.284 **	−2.801	−0.276 **	−2.737
CT	0.826 **	2.690	0.946 **	3.049	0.846 **	2.685	0.971 **	3.146	0.841 **	2.700

Table 6. *Cont.*

Variable	Base Model		Model 1 (50 m Buffer Zone)		Model 2 (100 m Buffer Zone)		Model 3 (150 m Buffer Zone)		Model 4 (200 m Buffer Zone)	
	Coefficient	*z*-Value	Coefficient	*z*-Value	Coefficient	*z*-Value	Coefficient	*z*-Value	Coefficient	*z*-Value
OA	0.019	1.856	0.026 *	2.505	0.024 *	2.276	0.011	1.023	0.025 *	1.966
FA	−0.007 **	−3.796	−0.009 **	−4.362	−0.008 **	−4.097	−0.008 **	−4.250	−0.009 **	−4.361
BSC	8.456 *	2.362	10.935 **	2.915	9.393 **	2.534	9.503 **	2.555	10.549 **	2.727
TDU	0.048 **	3.021	0.054 **	3.395	0.051 **	3.205	0.052 **	3.322	0.056 **	3.579
OSR			2.121	0.475	−3.632	−0.551	−5.264	−0.617	0.046	0.004
FAR			0.259	1.107	0.070	0.192	0.919 *	2.227	0.351	0.555
WSA			−21.772	−0.929	−1.802	−0.295	6.439 *	1.898	0.576	0.236
GSR			2.392	1.618	2.776	1.479	−4.695 **	−2.560	5.168	1.450
R-squared	0.377		0.395		0.390		0.418		0.406	
LL	−306.87		−306.452		−304.808		−301.600		−302.857	

Note: (1) LL means log likelihood; (2) * $p < 0.05$, ** $p < 0.01$.

Table 7. Comparison of regression results from spatial lag models of EUI_W.

Variable	Base Model		Model 1 (50 m Buffer Zone)		Model 2 (100 m Buffer Zone)		Model 3 (150 m Buffer Zone)		Model 4 (200 m Buffer Zone)	
	Coefficient	*z*-Value	Coefficient	*z*-Value	Coefficient	*z*-Value	Coefficient	*z*-Value	Coefficient	*z*-Value
Spatial lag	0.527 **	6.622	0.454 **	5.255	0.394 **	4.285	0.387 **	4.210	0.403 **	4.307
Constant	−60.536	−1.425	−30.816	−0.685	−18.328	−0.402	−43.028	−0.953	−32.874	−0.687
YB	0.034	1.575	0.020	−0.685	0.016	0.697	0.034	1.536	0.025	1.051
NF	−0.141 *	−1.900	−0.121	−1.522	−0.095	−1.257	−0.145	−1.881	−0.131	−1.689
CT	0.210	0.902	0.271	1.157	0.151	0.641	0.160	0.683	0.195	0.820
OA	0.004	0.530	0.011	1.333	0.008	0.989	−0.006	−0.743	0.002	0.199
FA	−0.003 *	−2.512	−0.005 **	−3.223	−0.004 **	−2.796	−0.007 **	−2.796	−0.004 **	−2.664
BSC	5.526 *	1.94	7.001 *	2.474	6.620 *	2.394	6.251 *	2.223	6.441 *	2.179
TDU	0.017	1.396	0.022	1.832	0.018	1.514	0.020	1.663	0.019	1.553
OSR			−2.550	−0.746	−9.249	−1.837	−19.288 **	−2.814	−13.746	−1.635
FAR			0.106	0.596	0.287	1.041	1.256 **	3.733	0.699	1.426
WSA			−17.379	−0.974	5.447	1.169	9.377 **	3.486	2.806	1.482
GSR			2.547 *	2.213	3.454 *	2.347	−2.021	−1.448	3.872	1.394
R-squared	0.413		0.432		0.442		0.454		0.432	
LL	−272.672		−268.946		−266.83		−265.266		−268.119	

Note: (1) LL means log likelihood; (2) * $p < 0.05$, ** $p < 0.01$.

3.3.1. Annual and Seasonal Regression Results for the Base Model

The winter electricity consumption model outperforms the summer model in terms of R-squares. Interestingly, this observation contrasts with previous research findings in hot summer/cold winter zones [24]. The limitations of the latter study were primarily due to its reliance on MLR without accounting for spatial autocorrelation. As presented in Figure 7c, the global Moran's I of EUI_W is the highest among three periods, registering at 0.494. Undoubtedly, this significantly inflates the correlation coefficients of the spatial lag variables, thereby influencing the model fit to some extent. According to Tables 5–7, it becomes evident that the spatial lag variables for EUI_A, EUI_S, and EUI_W exhibit highly significant impacts on the dependent variable ($p < 0.01$). Notably, during winter, the spatial lag variable demonstrates the highest correlation coefficient at 0.527, whereas for annual and summer models, it is 0.419 and 0.385, respectively. This not only explains the observed differences but also emphasizes the strength of this study. Specifically, SLR effectively mitigates spatial autocorrelation issues, resulting in more plausible and reasonable regression results.

Building upon this analysis, the base models are further assessed from a significance perspective. It is observed that, aside from spatial lag variables, only three variables exhibit significance in the winter base model, whereas the summer base model includes five significant variables. In hot summer/cold winter zones, cooling energy consumption remains the dominant energy demand, making it more susceptible to the influence of basic building data (control variables). Specifically, variables like *NF*, *CT*, *FA*, *BSC*, and

TDU emerge as the key factors affecting residential electricity consumption, aligning with established theories [24,25,73–75].

In this study, both *YB* and *OA* do not exhibit significant impacts on residential electricity consumption. This finding aligns with the results of Ref. [24], which primarily focused on newer buildings. By contrast, our study primarily investigates older buildings, with 95% of the samples constructed before 2000. During this period, differences in insulation and heat retention among buildings were relatively limited, as shown in Figure 5. Furthermore, our analysis indicates that roughly 70% of *OA* values were less than 30°, signifying that the majority of buildings primarily faced south. The limited variability among the samples contributes to the lack of statistical significance in the regression results for these variables.

3.3.2. Spatial Heterogeneity in the Impact of Urban Morphology on Energy Consumption

In this subsection, we investigate the heterogeneous characteristics of the impact of spatial morphology at different buffer scales on BEC during the same timeframe.

Figure 8 provides a statistical overview, with the line portion representing urban morphology variables and the bar section representing control variables in all models. Comparing control variables across the base models within the same group reveals minimal differences in these significance indicators, mostly staying within one indicator. This similarity, in alignment with the results of Ref. [25], illustrates the dependability of these comparative models. Overall, the count of statistically significant urban morphology variables exhibits significant spatial variation, even within the same timeframe. Consequently, the indiscriminate use of a single range for all indicators in spatial morphology regression analysis could lead to inaccurate results and potentially flawed conclusions.

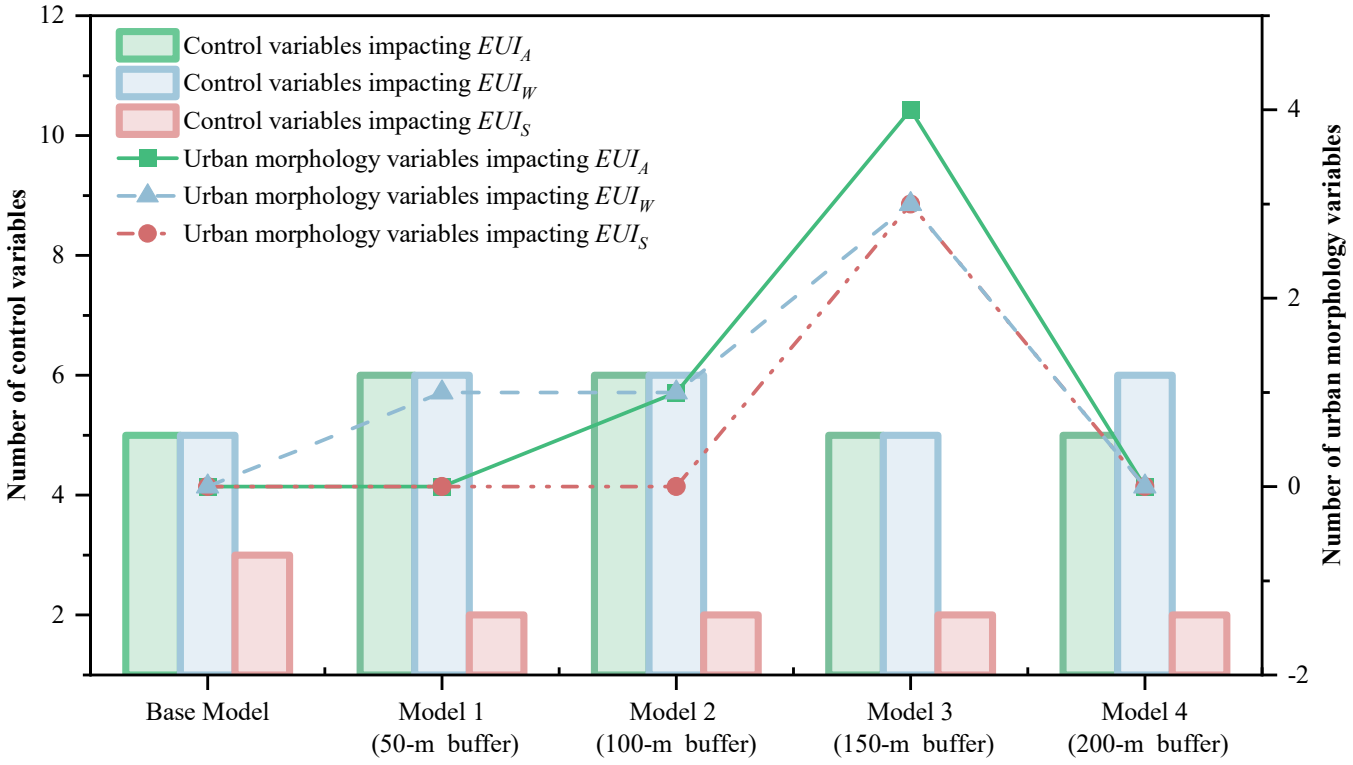

Figure 8. The number variation trend in building energy consumption impacting variables under different buffers.

As shown in Tables 5–7, the best model fit for EUI_A, EUI_S, and EUI_W is achieved with the 150 m buffer zone. A higher log likelihood (LL) value, indicating a larger log likelihood function, reflects greater model regression accuracy. During the entire year, all urban morphology variables in Model 3 exhibit significant correlations with BEC, as

depicted in Figure 9. Simultaneously, during seasonal periods, three out of the four urban morphology variables demonstrate significant correlations with BEC. However, when the buffer zone spatial scale reaches 200 m, none of the urban morphology variables for any time period exhibit statistical significance. Thus, it is evident that the effective influence of urban morphology on BEC in this study primarily occurs within a 150 m scale range.

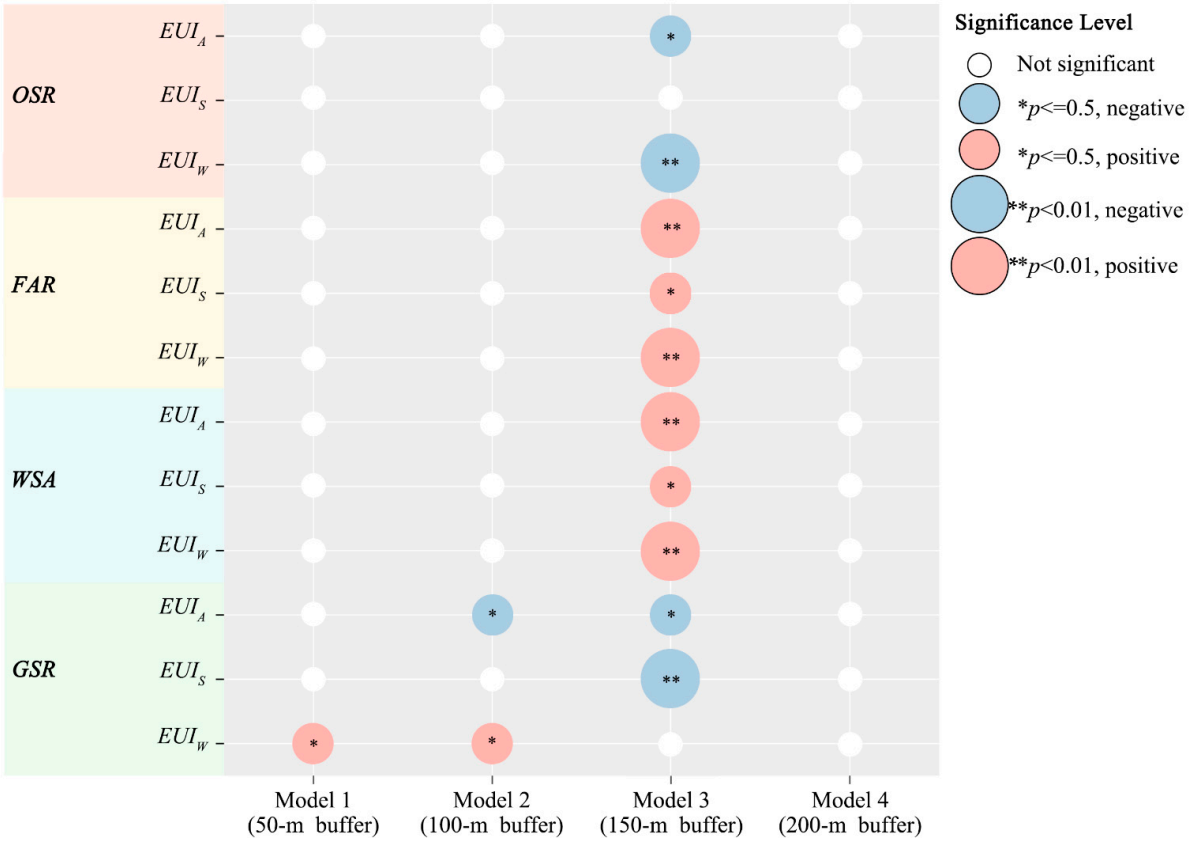

Figure 9. Comparison of the significance of urban morphology variables under different buffers.

Nevertheless, determining an appropriate spatial scale for building energy regression modeling remains challenging. Ref. [25] found that urban morphology significantly influences residential energy consumption within 50 m and 100 m radii in their study of Seattle. Furthermore, research from colder regions indicated that a 100 m neighborhood range had the most significant impact on BEC [34]. A more interesting result comes from Singapore, where Ref. [33] discovered that increasing the buffer zone size did not exhibit clear trends among variables, suggesting that spatial distance may not affect the model fit significantly. Indeed, regional disparities in climate, spatial morphology, energy consumption characteristics, and user behavior lead to significant variations in research findings. This underscores the context-specific nature of spatial morphology's influence on BEC across different urban areas. Blindly applying research results from one region to another for BEC modeling or policy development is not scientifically sound.

Incorporating insights from prior research, urban morphology indicators within a 150 m buffer zone can be employed to conduct spatial visualization modeling of BEC in old residential buildings on a local university campus. While this approach undeniably enhances the accuracy of BEC prediction models to some extent, it remains insufficient, as it might overlook significant indicators. In this study, for instance, *GSR* exhibited significance within 50~100 m range during the winter season, rather than within a 150 m radius. Additionally, over the course of the year, *GSR* displayed notable correlations with BEC within a 100 m buffer zone, and its z-value surpasses that of Model 3 (150 m), indicating increased significance. These variables fall outside the scope of a 150 m buffer zone. Lastly,

in terms of EUI_S, *OSR* failed to exhibit statistical significance within all buffer zone ranges. Prior research has emphasized that the inclusion of non-significant variables can impact model regression performance [23].

In summary, prior research has typically utilized a single buffer zone for regression analysis, which is inherently flawed. On one hand, while previous studies have demonstrated the optimal buffer zone size for fitting models to some extent, the heterogeneity in the impact of urban morphology across different regions implies that such findings cannot be universally applied. On the other hand, the significance of each urban morphological variable does indeed vary across different buffer zones, indicating that their spatial influence on BEC differs. This factor should be taken into account in the process of UBEC regression modeling.

3.3.3. Temporal Heterogeneity in the Impact of Urban Morphology on Energy Consumption

In this subsection, we explore the diverse impacts of urban morphology indicators within a consistent-scale buffer zone on BEC across different time periods.

Firstly, significant disparities are evident among urban morphology indicators (Figure 8). Within a 150 m buffer zone, the number of significant variables varies impacting EUI_A, EUI_S, and EUI_W. Even when the significant variables are consistent between summer and winter, their constituent variable types remain distinct. *OSR* lacks significance during summer but exhibits an opposite pattern during winter. Conversely, *GSR* lacks significance during winter but shows the opposite trend during summer. Furthermore, *WSA* and *FAR* significantly impact EUI_A, EUI_S, and EUI_W positively, while *OSR* consistently demonstrates a negative correlation. This suggests that higher *OSR* and lower *FAR* and *WSA* lead to reduced BEC. These indicators are closely associated with urban built environment intensity. As seen in Figure 6, Pearson correlation analysis reveals that cities with higher spatial intensity tend to have looser *OSR*, denser *FAR*, and larger *WSA*. Our findings support the idea that greater built environment intensity is positively correlated with BEC, in line with existing theories [24,76]. Chongqing, a high-density mountainous city, experiences exacerbated regional heat island effects [77], resulting in increased indoor cooling energy use during the summer. Notably, we also observe a significant negative impact of high-intensity built environments on EUI_W, consistent with findings from Ref. [19] in a similar climate zone. Nevertheless, previous research has also suggested that higher-density communities are linked to reduced winter heat loss [78]. Differences may arise from variations in construction intensity near the samples. Unlike U.S.-based studies primarily focusing on single-family residences, our samples consist of slab and tower apartments in densely populated mountainous urban communities. During the winter, more compact and densely built spaces, influenced by topography, may increase mutual shading, substantially reducing the solar heating effect of buildings.

Furthermore, even the same indicators may simultaneously manifest entirely distinct positive and negative effects. Specifically, *GSR* within a 100 m buffer zone demonstrates a significant negative correlation with EUI_A, yet it manifests a significant positive correlation with EUI_W. This interesting phenomenon underscores the dual impact of vegetation on BEC [25]. During summer, trees provide shading, reducing direct sunlight exposure on building surfaces [79]. Moreover, the evaporative cooling effect lowers ambient temperatures near buildings [80], significantly decreasing BEC in hot summer/cold winter zones. However, during winter, the tree canopy may obstruct the penetration of warm sunlight to building exteriors. This implies that the building's walls and roof cannot benefit from the heating effect of sunlight, increasing the workload of the heating system. From an annual perspective, a study from a hot summer/cold winter zone aligns with our findings [24], as, in these areas, EUI_S dominates. Additionally, a case study in Harbin, China, supports this perspective [23], confirming that areas with less greenery tend to experience warmer winters.

In summary, spatial morphology indeed exerts heterogeneous effects on BEC across distinct temporal segments. This heterogeneity can be categorized into three facets. First, despite identical spatial scales, the number of significant urban morphology indicators

varies across different time periods. Second, even when the quantity of significant indicators remains constant, their types differ between various time periods. Third, the direction and pathway of their effects vary across different time periods, consistent with the number and types of significant indicators.

3.4. Proposition and Application of a Three-Tiered Framework for Planning Processes

Section 3.3 provides a detailed demonstration of how urban morphology indeed exerts spatio-temporal heterogeneity effects on BEC. This phenomenon poses challenges to urban building energy model construction, as users must make inferences about unknown model parameters. This challenge is compounded by the diversity in building project categories and the inherent complexity and uncertainty in urban morphology parameters [1]. In larger urban contexts, this uncertainty can be amplified [81]. The spatio-temporal heterogeneity in the influence of urban morphology on BEC constitutes a significant source of complexity in data-intensive processes. Therefore, it is vital to identify the most influential attributes to provide effective environmental and cost feedback and simplify urban building decision making. This paper proposes a context-specific, region-level urban energy consumption modeling integration framework, aiming to establish a parameter repository connecting morphological indicators, spatial boundaries, and energy consumption periods across diverse regions. It facilitates precise modeling and visual comparative analysis of UBEC, enabling urban planners to coordinate and manage key initiatives.

Figure 10 illustrates this framework, comprising three components: macro-level urban project decomposition, the construction of a key urban morphology indicator database, and spatial BEC comparisons within a specific context.

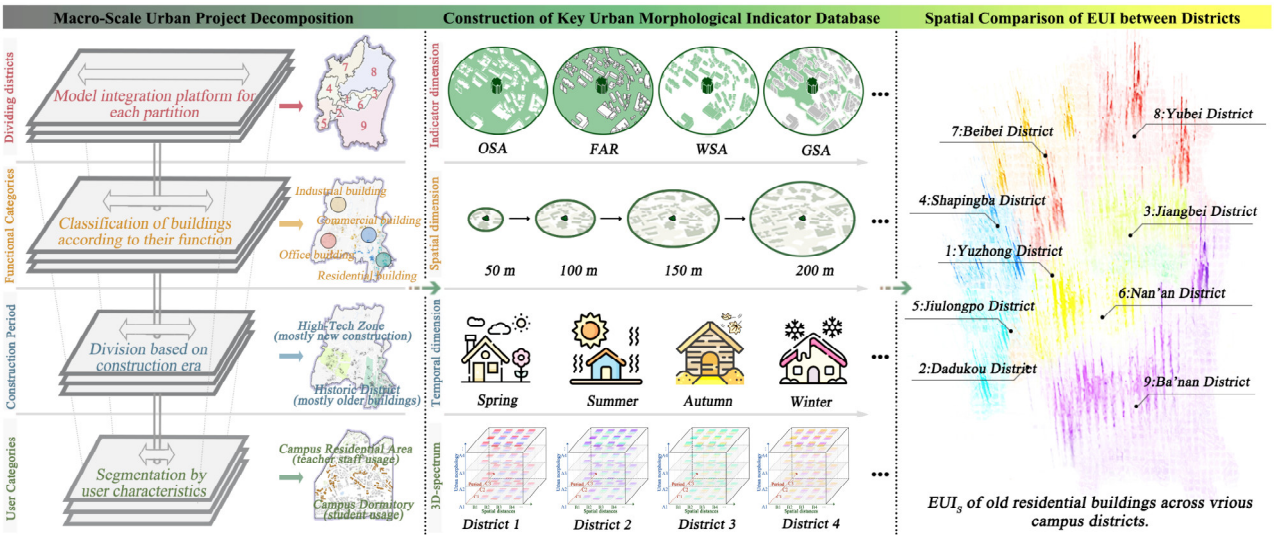

Figure 10. Three-tiered framework for planning processes.

Firstly, due to the multitude of factors affecting UBEC, macro-level project decomposition is necessary. This ensures consistency in background variables while setting a specific scenario. After constructing a modeling integration platform for each region, classification is based on local building characteristics, forming a crucial foundation for precise modeling. Figure 10 shows three standard criteria for specialized classification modeling: functional types (residential, commercial, office, industrial), historical characteristics (old neighborhoods, high-tech zones), and user characteristics (teachers, students). This paper primarily focuses on specialized analysis of old residential buildings within campus settings, with teaching staff as users. As research on UBEC advances, specialized energy consumption analysis within specific scenarios gains traction. Similarly, in the context of campus buildings, Ref. [28] places heightened emphasis on the impact of urban morphology on dormitory energy consumption characteristics, with students as users.

Therefore, if target projects in a region reach a certain scale and have statistical significance, these classification criteria can be flexibly configured and combined. As information on specialized energy consumption models of various types continues to expand, the regional integration platform will progressively improve, prioritizing the coverage of buildings with similar attributes.

Secondly, from the perspectives of spatial boundaries, energy consumption periods, and morphological indicators, the construction of a database of key urban morphology indicators for different projects is initiated. By eliminating spatial autocorrelation and conducting multi-model comparative experiments, key urban morphology indicators in different periods and their primary impact boundaries can be identified. The creation of the 3D spectrum enables precise observation of how urban morphology impacts specific objects, facilitating the balancing of energy consumption characteristics in different periods and targeted optimization of project boundaries within urban renewal plans.

Finally, a model for predicting regional BEC is constructed to enable spatial visual comparisons of specialized energy consumption. Following the identification of key parameters influencing BEC in the second step, along with their corresponding significant periods and spatial scales, methods such as typology, multivariate regression, and machine learning can be employed for UBEC prediction [51,82,83]. This assists energy managers in accurately understanding specialized electricity demands and enables the integration of BEC data with different attribute characteristics, enhancing the information quality of the database and regional comparability. Urban stakeholders can use the regionalized BEC integration platform to clearly delineate differences in BEC spatial distribution on a regional basis, facilitating transparent management and energy policy formulation for areas with weak specialized energy consumption. Based on the regional BEC integration platform, long-term dynamic monitoring of key indicators can be implemented for projects with excessively high energy consumption, allowing for real-time and flexible updates of specialized energy plans and enhancing overall energy efficiency.

3.5. Limitations and Prospects

This study acquired comprehensive basic information on old residential buildings within a campus, along with their energy consumption data. However, the limited sample size currently hinders our ability to construct a predictive urban energy consumption model. Additionally, the distinct differences observed in spatial lag variables across various time periods within the SLM prevent a straightforward assessment of BEC contributions through coefficient comparisons. Notwithstanding these limitations, this endeavor nonetheless furnishes a detailed demonstration of the heterogeneity in the impact of urban morphology on BEC. The inclusion of these significant spatial indicators can substantially enhance the accuracy of BEC modeling across different timeframes. As noted by Ref. [84], urban design and planning methodologies must adapt to the evolving urban and suburban. In fact, the work reported here represents an inaugural step in a cohesive research initiative. In accordance with the framework established in Section 3.4, this paper intends to collect residential building information from other campuses in the future, aiming to create a "Campus Residential Building Energy Data Platform" for mountainous cities.

The findings in Section 3.3 support the argument that employing only a single buffer zone for regression analysis is inherently imprecise and may inadvertently omit crucial indicators. Nevertheless, this approach is commonly adopted in existing research studies [23,29]. Therefore, this study recommends that future reports consider expanding beyond the examination of urban morphology within the 50~200 m range and explore larger urban scales as needed. Furthermore, it is essential to incorporate significant factors between different buffer zones into a unified model. In theory, this would significantly enhance the accuracy of model regression and render it more rational. This approach underscores the significance of constructing a database of key indicators within the framework proposed in this paper.

Lastly, this study has explored four urban morphology indicators and has yet to investigate other urban indicators such as waterbody ratios, land use, and road density. Given the inherent complexity of actual urban morphology, future research can include a more extensive array of indicators to reflect real urban morphology characteristics. This will facilitate a more comprehensive exploration of the spatio-temporal heterogeneity in BEC impacts, thereby improving the precision of regression models.

4. Conclusions

Adjusting urban morphology at the neighborhood level to formulate energy-saving plans and renewable energy strategies is a widely recognized approach. However, in the process of formulating specialized energy-saving planning strategies, we still struggle to determine the appropriate actions to reduce the BEC of target buildings [1]. This challenge largely stems from the seasonal characteristics of BEC and spatial scale diversity. This study, using old campus residential buildings as an example and considering spatial autocorrelation, meticulously examines the influence of four different urban morphology scales (50~200 m) on BEC during three time periods: the entire year, summer, and winter. The research results provide compelling evidence that urban morphology exhibits pronounced spatio-temporal heterogeneity in BEC within the neighborhood. The following conclusions are drawn:

- Annual and seasonal SLMs perform best within a 150 m buffer zone. However, not all significant indicators are within this spatial range. Blindly employing a single range for all indicators in urban morphology regression analyses may result in inaccuracies and even erroneous inferences.
- During the annual, summer, and winter periods, *GSR* demonstrates significant correlations with BEC within buffer zone ranges of 150 m, 50~100 m, and 100 m, respectively.
- When the spatial scale remains the same but the energy consumption period differs, significant urban morphology indicators exhibit differences in terms of quantity, category, and polarity.
- *GSR* has a pronounced dual impact on BEC, showing a significant negative correlation with EUI_A but a significant positive correlation with EUI_W.
- Neighborhoods with larger *OSR*, smaller *FAR*, and lower *WSA* experience a reduction in EUI_A of old residential buildings.

Generally, this strong heterogeneity is widespread and inherent. The diversity in building project categories and urban spatial categories may further contribute to the spatio-temporal heterogeneity of urban morphology's impact on BEC. Importantly, key urban morphology indicators affecting BEC are often difficult to predict. Therefore, a framework is proposed for constructing an indicator database that links form indicators, spatial boundaries, and energy consumption periods. By establishing specialized 3D spectrums, this framework facilitates the observation of urban morphology impact pathways in specific scenarios, allowing for the optimization of urban morphology boundaries across different time periods. It can also be used to construct regional UBEC prediction models. To sum up, this study provides a vital reference for understanding the spatio-temporal heterogeneity of urban morphology's impact on BEC and offers a comprehensive framework to address this issue, enabling the implementation of efficient and effective energy measures.

Author Contributions: Conceptualization, J.M. and H.H.; methodology, Y.Z.; software, J.M.; validation, J.M., Y.Z. and M.P.; formal analysis, J.M.; investigation, J.M.; resources, H.H.; data curation, J.M. and H.H.; writing—original draft preparation, J.M.; writing—review and editing, H.H.; visualization, J.M.; supervision, H.H. and M.P.; project administration, H.H. and M.P.; funding acquisition, H.H. and M.P. All authors have read and agreed to the published version of the manuscript.

Funding: This study is funded by the National Natural Science Foundation of China (No. 52078071) and the Natural Science Foundation of Chongqing (No. CSTB2023NSCQ-MSX0801).

Data Availability Statement: The data presented in this study are available on request from the corresponding author. The data are not publicly available due to their large volume.

Conflicts of Interest: The authors declare no conflicts of interest.

Nomenclature

BEC	Building energy consumption	MLR	Multiple linear regression
UBEC	Urban building energy consumption	SLM	Spatial lag model
YB	Year built	SEM	Spatial error model
NF	Number of floors	OSR	Open space ratio
CT	Contiguity type	FAR	Floor area ratio
OA	Orientation angle	WSA	Total wall surface area
FA	Floor area	GSR	Green space ratio
BSC	Building shape coefficient	EUI_A	Annual energy use intensity
TDU	Total number of dwelling units	EUI_S	Summer energy use intensity
EUI	Energy usage intensity	EUI_W	Winter energy use intensity
AIC	Akaike information criterion	SC	Schwarz criterion
LL	Log likelihood	LM	Lagrange multiplier

Notes

[1] Over the past 50 years, in China's hot summer/cold winter zones, the standards for residential energy-efficient design have evolved, including "*GB 50176-1986 Code for Thermal Design of Civil Building*", "*GB 50176-1993 Code for Thermal Design of Civil Building*", " *JGJ 134-2001 Design Standard for Energy Efficiency of Residential Buildings in Hot Summer and Cold Winter Areas*", and "*JGJ 134-2010 Design Standard for Energy Efficiency of Residential Buildings in Hot Summer and Cold Winter Areas*" [15,48–50]. It is important to note that when new regulations are introduced, previous standards of the same type are rendered obsolete and are no longer in effect, following the guidelines of the Ministry of Housing and Urban-Rural Development of the People's Republic of China.

References

1. Cajot, S.; Peter, M.; Bahu, J.-M.; Guignet, F.; Koch, A.; Maréchal, F. Obstacles in Energy Planning at the Urban Scale. *Sustain. Cities Soc.* **2017**, *30*, 223–236. [CrossRef]
2. Li, C.; Hong, T.; Yan, D. An Insight into Actual Energy Use and Its Drivers in High-Performance Buildings. *Appl. Energy* **2014**, *131*, 394–410. [CrossRef]
3. Quan, S.J.; Li, C. Urban Form and Building Energy Use: A Systematic Review of Measures, Mechanisms, and Methodologies. *Renew. Sustain. Energy Rev.* **2021**, *139*, 110662. [CrossRef]
4. Rathnayake, H.; Mizunoya, T. A Study on GHG Emission Assessment in Agricultural Areas in Sri Lanka: The Case of Mahaweli H Agricultural Region. *Environ. Sci. Pollut. Res.* **2023**, *30*, 88180–88196. [CrossRef] [PubMed]
5. Zhu, W.; Yuan, C. Urban Heat Health Risk Assessment in Singapore to Support Resilient Urban Design-By Integrating Urban Heat and the Distribution of the Elderly Population. *Cities* **2023**, *132*, 104103. [CrossRef]
6. Zhang, Q.; Li, J. Building Carbon Peak Scenario Prediction in China Using System Dynamics Model. *Environ. Sci. Pollut. Res.* **2023**, *30*, 96019–96039. [CrossRef]
7. Mariano-Hernández, D.; Hernández-Callejo, L.; Zorita-Lamadrid, A.; Duque-Pérez, O.; Santos García, F. A Review of Strategies for Building Energy Management System: Model Predictive Control, Demand Side Management, Optimization, and Fault Detect & Diagnosis. *J. Build. Eng.* **2021**, *33*, 101692. [CrossRef]
8. Moshari, A.; Aslani, A.; Zolfaghari, Z.; Malekli, M.; Zahedi, R. Forecasting and Gap Analysis of Renewable Energy Integration in Zero Energy-Carbon Buildings: A Comprehensive Bibliometric and Machine Learning Approach. *Environ. Sci. Pollut. Res.* **2023**, *30*, 91729–91745. [CrossRef]
9. Liu, K.; Xu, X.; Zhang, R.; Kong, L.; Wang, W.; Deng, W. Impact of Urban Form on Building Energy Consumption and Solar Energy Potential: A Case Study of Residential Blocks in Jianhu, China. *Energy Build.* **2023**, *280*, 112727. [CrossRef]
10. Fracastoro, G.V.; Serraino, M. A Methodology for Assessing the Energy Performance of Large Scale Building Stocks and Possible Applications. *Energy Build.* **2011**, *43*, 844–852. [CrossRef]
11. Lin, Q.; Liu, K.; Hong, B.; Xu, X.; Chen, J.; Wang, W. A Data-Driven Framework for Abnormally High Building Energy Demand Detection with Weather and Block Morphology at Community Scale. *J. Clean. Prod.* **2022**, *354*, 131602. [CrossRef]
12. Torabi Moghadam, S.; Coccolo, S.; Mutani, G.; Lombardi, P.; Scartezzini, J.-L.; Mauree, D. A New Clustering and Visualization Method to Evaluate Urban Heat Energy Planning Scenarios. *Cities* **2019**, *88*, 19–36. [CrossRef]
13. Li, D.; He, J.; Li, L. A Review of Renewable Energy Applications in Buildings in the Hot-Summer and Warm-Winter Region of China. *Renew. Sust. Energ. Rev.* **2016**, *57*, 327–336. [CrossRef]
14. Merabet, G.H.; Essaaidi, M.; Ben Haddou, M.; Qolomany, B.; Qadir, J.; Anan, M.; Al-Fuqaha, A.; Abid, M.R.; Benhaddou, D. Intelligent Building Control Systems for Thermal Comfort and Energy-Efficiency: A Systematic Review of Artificial Intelligence-

Assisted Techniques. *Renew. Sust. Energ. Rev.* **2021**, *144*, 11096, Erratum in *Renew. Sust. Energ. Rev.* **2021**, *145*, 111116. [CrossRef]
15. *JGJ 134-2010*; Design Standard for Energy Efficiency of Residential Buildings in Hot Summer and Cold Winter Areas. China Architecture & Building Press: Beijing, China, 2010.
16. *GB 50189-2015*; Design Standard for Energy Efficiency of Public Buildings. China Architecture & Building Press: Beijing, China, 2015.
17. *GB 50176-2016*; Thermal Design Code for Civil Building. China Architecture & Building Press: Beijing, China, 2016.
18. Tsirigoti, D.; Bikas, D. A Cross Scale Analysis of the Relationship between Energy Efficiency and Urban Morphology in the Greek City Context. *Procedia Environ. Sci.* **2017**, *38*, 682–687. [CrossRef]
19. Zhang, M.; Gao, Z. Effect of urban form on microclimate and energy loads: Case study of generic residential district prototypes in Nanjing, China. *Sustain. Cities Soc.* **2021**, *70*, 102930. [CrossRef]
20. Ishii, S.; Tabushi, S.; Aramaki, T.; Hanaki, K. Impact of Future Urban Form on the Potential to Reduce Greenhouse Gas Emissions from Residential, Commercial and Public Buildings in Utsunomiya, Japan. *Energy Policy* **2010**, *38*, 4888–4896. [CrossRef]
21. Strømann-Andersen, J.; Sattrup, P.A. The Urban Canyon and Building Energy Use: Urban Density versus Daylight and Passive Solar Gains. *Energy Build.* **2011**, *43*, 2011–2020. [CrossRef]
22. Silva, M.; Oliveira, V.; Leal, V. Urban Form and Energy Demand: A Review of Energy-Relevant Urban Attributes. *J. Plan. Lit.* **2017**, *32*, 346–365. [CrossRef]
23. Leng, H.; Chen, X.; Ma, Y.; Wong, N.H.; Ming, T. Urban Morphology and Building Heating Energy Consumption: Evidence from Harbin, a Severe Cold Region City. *Energy Build.* **2020**, *224*, 110143. [CrossRef]
24. Li, C.; Song, Y.; Kaza, N. Urban Form and Household Electricity Consumption: A Multilevel Study. *Energy Build.* **2018**, *158*, 181–193. [CrossRef]
25. Ahn, Y.; Sohn, D.-W. The Effect of Neighbourhood-Level Urban Form on Residential Building Energy Use: A GIS-Based Model Using Building Energy Benchmarking Data in Seattle. *Energy Build.* **2019**, *196*, 124–133. [CrossRef]
26. Taleghani, M.; Tenpierik, M.; van den Dobbelsteen, A.; de Dear, R. Energy Use Impact of and Thermal Comfort in Different Urban Block Types in the Netherlands. *Energy Build.* **2013**, *67*, 166–175. [CrossRef]
27. Vartholomaios, A. A Parametric Sensitivity Analysis of the Influence of Urban Form on Domestic Energy Consumption for Heating and Cooling in a Mediterranean City. *Sustain. Cities Soc.* **2017**, *28*, 135–145. [CrossRef]
28. Xie, M.; Wang, M.; Zhong, H.; Li, X.; Li, B.; Mendis, T.; Xu, S. The Impact of Urban Morphology on the Building Energy Consumption and Solar Energy Generation Potential of University Dormitory Blocks. *Sustain. Cities Soc.* **2023**, *96*, 104644. [CrossRef]
29. Wong, N.H.; Jusuf, S.K.; Syafii, N.I.; Chen, Y.; Hajadi, N.; Sathyanarayanan, H.; Manickavasagam, Y.V. Evaluation of the Impact of the Surrounding Urban Morphology on Building Energy Consumption. *Sol. Energy* **2011**, *85*, 57–71. [CrossRef]
30. Zhu, S.; Li, Y.; Wei, S.; Wang, C.; Zhang, X.; Jin, X.; Zhou, X.; Shi, X. The Impact of Urban Vegetation Morphology on Urban Building Energy Consumption during Summer and Winter Seasons in Nanjing, China. *Landsc. Urban Plan.* **2022**, *228*, 104576. [CrossRef]
31. Wang, W.; Lin, Q.; Chen, J.; Li, X.; Sun, Y.; Xu, X. Urban Building Energy Prediction at Neighborhood Scale. *Energy Build.* **2021**, *251*, 111307. [CrossRef]
32. Oraiopoulos, A.; Howard, B. On the Accuracy of Urban Building Energy Modelling. *Renew. Sustain. Energy Rev.* **2022**, *158*, 111976. [CrossRef]
33. Neo, H.Y.R.; Wong, N.H.; Ignatius, M.; Yuan, C.; Xu, Y.; Cao, K. Spatial Analysis of Public Residential Housing's Electricity Consumption in Relation to Urban Landscape and Building Characteristics: A Case Study in Singapore. *Energy Environ.* **2023**, *34*, 233–254. [CrossRef]
34. Chen, X.; Leng, H.; Ma, Y. Scale Identification and Mechanism Analysis of Harbin Urban Block Morphology Affecting Building Energy Consumption in Severe Cold Regions. *Ind. Build.* **2023**, *53*, 91–95. (In Chinese)
35. Kazmi, H.; Fu, C.; Miller, C. Ten Questions Concerning Data-Driven Modelling and Forecasting of Operational Energy Demand at Building and Urban Scale. *Build. Environ.* **2023**, *239*, 110407. [CrossRef]
36. Torabi Moghadam, S.; Delmastro, C.; Corgnati, S.P.; Lombardi, P. Urban Energy Planning Procedure for Sustainable Development in the Built Environment: A Review of Available Spatial Approaches. *J. Clean. Prod.* **2017**, *165*, 811–827. [CrossRef]
37. Ziwei, L.; Borong, L.; Shanwen, Z.; Yanchen, L.; Zhe, W.; Jian, D. A Review of Operational Energy Consumption Calculation Method for Urban Buildings. *Build. Simul.* **2020**, *13*, 739–751. [CrossRef]
38. Zhao, H.; Magoulès, F. A Review on the Prediction of Building Energy Consumption. *Renew. Sustain. Energy Rev.* **2012**, *16*, 3586–3592. [CrossRef]
39. Lu, Y.; Chen, Q.; Yu, M.; Wu, Z.; Huang, C.; Fu, J.; Yu, Z.; Yao, J. Exploring Spatial and Environmental Heterogeneity Affecting Energy Consumption in Commercial Buildings Using Machine Learning. *Sustain. Cities Soc.* **2023**, *95*, 104586. [CrossRef]
40. Ohlsson, K.E.A.; Olofsson, T. Benchmarking the Practice of Validation and Uncertainty Analysis of Building Energy Models. *Renew. Sustain. Energy Rev.* **2021**, *142*, 110842. [CrossRef]
41. Hong, T.; Chen, Y.; Luo, X.; Luo, N.; Lee, S.H. Ten Questions on Urban Building Energy Modeling. *Build. Environ.* **2020**, *168*, 106508. [CrossRef]
42. Jin, X.; Zhang, C.; Xiao, F.; Li, A.; Miller, C. A Review and Reflection on Open Datasets of City-Level Building Energy Use and Their Applications. *Energy Build.* **2023**, *285*, 112911. [CrossRef]

43. Yang, X.; Peng, L.L.H.; Jiang, Z.; Chen, Y.; Yao, L.; He, Y.; Xu, T. Impact of Urban Heat Island on Energy Demand in Buildings: Local Climate Zones in Nanjing. *Appl. Energy* **2020**, *260*, 114279. [CrossRef]
44. Kottek, M.; Grieser, J.; Beck, C.; Rudolf, B.; Rubel, F. World Map of the Köppen-Geiger Climate Classification Updated. *Meteorol. Z.* **2006**, *15*, 259–263. [CrossRef] [PubMed]
45. Jones, R.V.; Fuertes, A.; Lomas, K.J. The Socio-Economic, Dwelling and Appliance Related Factors Affecting Electricity Consumption in Domestic Buildings. *Renew. Sustain. Energy Rev.* **2015**, *43*, 901–917. [CrossRef]
46. Swan, L.G.; Ugursal, V.I. Modeling of End-Use Energy Consumption in the Residential Sector: A Review of Modeling Techniques. *Renew. Sustain. Energy Rev.* **2009**, *13*, 1819–1835. [CrossRef]
47. Brøgger, M.; Wittchen, K.B. Estimating the Energy-Saving Potential in National Building Stocks—A Methodology Review. *Renew. Sustain. Energy Rev.* **2018**, *82*, 1489–1496. [CrossRef]
48. *GB 50176-1986*; Thermal Design Code for Civil Building. China Architecture & Building Press: Beijing, China, 1986.
49. *GB 50176-1993*; Thermal Design Code for Civil Building. China Architecture & Building Press: Beijing, China, 1993.
50. *JGJ 134-2001*; Design Standard for Energy Efficiency of Residential Buildings in Hot Summer and Cold Winter Areas. China Architecture & Building Press: Beijing, China, 2001.
51. Torabi Moghadam, S.; Toniolo, J.; Mutani, G.; Lombardi, P. A GIS-Statistical Approach for Assessing Built Environment Energy Use at Urban Scale. *Sustain. Cities Soc.* **2018**, *37*, 70–84. [CrossRef]
52. McLoughlin, F.; Duffy, A.; Conlon, M. Characterising Domestic Electricity Consumption Patterns by Dwelling and Occupant Socio-Economic Variables: An Irish Case Study. *Energy Build.* **2012**, *48*, 240–248. [CrossRef]
53. Caputo, P.; Costa, G.; Ferrari, S. A Supporting Method for Defining Energy Strategies in the Building Sector at Urban Scale. *Energy Policy* **2013**, *55*, 261–270. [CrossRef]
54. Camporeale, P.E.; Mercader-Moyano, P. A GIS-Based Methodology to Increase Energy Flexibility in Building Cluster through Deep Renovation: A Neighborhood in Seville. *Energy Build.* **2021**, *231*, 110573. [CrossRef]
55. Aksoezen, M.; Daniel, M.; Hassler, U.; Kohler, N. Building Age as an Indicator for Energy Consumption. *Energy Build.* **2015**, *87*, 74–86. [CrossRef]
56. Abanda, F.H.; Byers, L. An Investigation of the Impact of Building Orientation on Energy Consumption in a Domestic Building Using Emerging BIM (Building Information Modelling). *Energy* **2016**, *97*, 517–527. [CrossRef]
57. Vandenbogaerde, L.; Verbeke, S.; Audenaert, A. Optimizing Building Energy Consumption in Office Buildings: A Review of Building Automation and Control Systems and Factors Influencing Energy Savings. *J. Build. Eng.* **2023**, *76*, 107233. [CrossRef]
58. Braulio-Gonzalo, M.; Juan, P.; Bovea, M.D.; Jose Rua, M. Modelling Energy Efficiency Performance of Residential Building Stocks Based on Bayesian Statistical Inference. *Environ. Modell. Softw.* **2016**, *83*, 198–211. [CrossRef]
59. Li, X.; Ying, Y.; Xu, X.; Wang, Y.; Hussain, S.A.; Hong, T.; Wang, W. Identifying Key Determinants for Building Energy Analysis from Urban Building Datasets. *Build. Environ.* **2020**, *181*, 107114. [CrossRef]
60. Wei, R.; Song, D.; Wong, N.H.; Martin, M. Impact of Urban Morphology Parameters on Microclimate. *Procedia Eng.* **2016**, *169*, 142–149. [CrossRef]
61. Liu, X.; Ming, Y.; Liu, Y.; Yue, W.; Han, G. Influences of Landform and Urban Form Factors on Urban Heat Island: Comparative Case Study between Chengdu and Chongqing. *Sci. Total Environ.* **2022**, *820*, 153395. [CrossRef] [PubMed]
62. Javanroodi, K.; Mahdavinejad, M.; Nik, V.M. Impacts of Urban Morphology on Reducing Cooling Load and Increasing Ventilation Potential in Hot-Arid Climate. *Appl. Energy* **2018**, *231*, 714–746. [CrossRef]
63. Shi, Q.; Liu, M.; Marinoni, A.; Liu, X. UGS-1m: Fine-Grained Urban Green Space Mapping of 31 Major Cities in China Based on the Deep Learning Framework. *Earth Syst. Sci. Data* **2023**, *15*, 555–577. [CrossRef]
64. Fan, X.L.; Luo, T.; Zhang, X.W.; Wu, L.L. Correlation between Urban Spatial Form and Residential Building Energy Use of Towns on a Continuous Scale: A Case of Changxing, Zhejiang and Lianjiang County, Fujian. *Acta Ecol. Sin.* **2022**, *42*, 3155–3166. (In Chinese)
65. Ha, J.; Kambe, M.; Pe, J. *Data Mining: Concepts and Techniques*; Elsevier: Amsterdam, The Netherlands, 2011. [CrossRef]
66. Erkuş, E.C.; Purutçuoğlu, V. Outlier Detection and Quasi-Periodicity Optimization Algorithm: Frequency Domain Based Outlier Detection (FOD). *Eur. J. Oper. Res.* **2021**, *291*, 560–574. [CrossRef]
67. Tso, G.K.F.; Guan, J. A Multilevel Regression Approach to Understand Effects of Environment Indicators and Household Features on Residential Energy Consumption. *Energy* **2014**, *66*, 722–731. [CrossRef]
68. Guo, R.; Li, N.; Mu, H.; Zhang, M.; Yang, X.; Han, Y.; Yao, R.; Shao, Z. Study on the Impact of Comprehensive Urbanization on Urban Civil Building CO2 Emissions in China. *Environ. Sci. Pollut. Res.* **2022**, *29*, 17709–17722. [CrossRef] [PubMed]
69. Dong, Y.-H.; Peng, F.-L.; Li, H.; Men, Y.-Q. Spatial Autocorrelation and Spatial Heterogeneity of Underground Parking Space Development in Chinese Megacities Based on Multisource Open Data. *Appl. Geogr.* **2023**, *153*, 102897. [CrossRef]
70. Anselin, L.; Bera, A. Spatial Dependence in Linear Regression Models with an Introduction to Spatial Econometrics. In *Handbook of Applied Economic Statistics*; CRC Press: New York, NY, USA, 1998; pp. 257–259, ISBN 978-0-429-17738-5.
71. Wiedenhofer, D.; Lenzen, M.; Steinberger, J.K. Energy Requirements of Consumption: Urban Form, Climatic and Socio-Economic Factors, Rebounds and Their Policy Implications. *Energy Policy* **2013**, *63*, 696–707. [CrossRef]
72. Fotheringham, A.S.; Brunsdon, C.; Charlton, M. *Geographically Weighted Regression: The Analysis of Spatially Varying Relationships*; John Wiley & Sons: New York, NY, USA, 2003; ISBN 0-470-85525-8.

73. Scott, F.L.; Jones, C.R.; Webb, T.L. What Do People Living in Deprived Communities in the UK Think about Household Energy Efficiency Interventions? *Energy Policy* **2014**, *66*, 335–349. [CrossRef]
74. Esmaeilimoakher, P.; Urmee, T.; Pryor, T.; Baverstock, G. Identifying the Determinants of Residential Electricity Consumption for Social Housing in Perth, Western Australia. *Energy Build.* **2016**, *133*, 403–413. [CrossRef]
75. Xu, X.; Xiao, B.; Li, C.Z. Critical Factors of Electricity Consumption in Residential Buildings: An Analysis from the Point of Occupant Characteristics View. *J. Clean. Prod.* **2020**, *256*, 120423. [CrossRef]
76. Tran, D.X.; Pla, F.; Latorre-Carmona, P.; Myint, S.W.; Caetano, M.; Kieu, H.V. Characterizing the Relationship between Land Use Land Cover Change and Land Surface Temperature. *ISPRS J. Photogramm. Remote Sens.* **2017**, *124*, 119–132. [CrossRef]
77. Huang, H.; Ma, J.; Yang, Y. Spatial Heterogeneity of Driving Factors for Urban Heat Health Risk in Chongqing, China: A New Identification Method and Proposal of Planning Response Framework. *Ecol. Indic.* **2023**, *153*, 110449. [CrossRef]
78. Ewing, R.; Rong, F. The Impact of Urban Form on U.S. Residential Energy Use. *Hous. Policy Debate* **2008**, *19*, 1–30. [CrossRef]
79. Yu, H.; Zhang, T.; Fukuda, H.; Ma, X. The Effect of Landscape Configuration on Outdoor Thermal Environment: A Case of Urban Plaza in Xi'An, China. *Build. Environ.* **2023**, *231*, 110027. [CrossRef]
80. Sanusi, R.; Johnstone, D.; May, P.; Livesley, S.J. Microclimate Benefits That Different Street Tree Species Provide to Sidewalk Pedestrians Relate to Differences in Plant Area Index. *Landsc. Urban Plan.* **2017**, *157*, 502–511. [CrossRef]
81. Demir Dilsiz, A.; Ng, K.; Kämpf, J.; Nagy, Z. Ranking Parameters in Urban Energy Models for Various Building Forms and Climates Using Sensitivity Analysis. *Build. Simul.* **2022**, *16*, 1587–1600. [CrossRef]
82. Costanzo, V.; Yao, R.; Li, X.; Liu, M.; Li, B. A Multi-Layer Approach for Estimating the Energy Use Intensity on an Urban Scale. *Cities* **2019**, *95*, 102467. [CrossRef]
83. Tian, W.; Zhu, C.; Sun, Y.; Li, Z.; Yin, B. Energy Characteristics of Urban Buildings: Assessment by Machine Learning. *Build. Simul.* **2021**, *14*, 179–193. [CrossRef]
84. Barnett, J. Redesigning the Metropolisthe Case for a New Approach. *J. Am. Plan. Assoc.* **1989**, *55*, 131–135. [CrossRef]